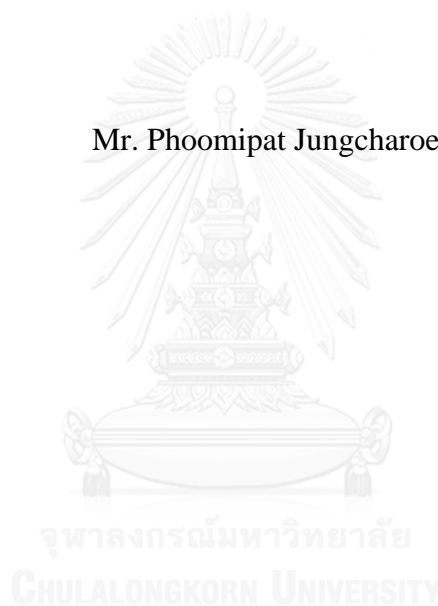


Synthesis of Nanoscale Zerovalent Iron (nZVI)  
Derived from Lignin Containing Wastewater for Arsenic Removal

Mr. Phoomipat Jungcharoen



บทคัดย่อและแฟ้มข้อมูลฉบับเต็มของวิทยานิพนธ์ตั้งแต่ปีการศึกษา 2554 ที่ให้บริการในคลังปัญญาจุฬาฯ (CUIR)  
เป็นแฟ้มข้อมูลของนิสิตเจ้าของวิทยานิพนธ์ ที่ส่งผ่านทางบัณฑิตวิทยาลัย

The abstract and full text of theses from the academic year 2011 in Chulalongkorn University Intellectual Repository (CUIR)  
are the thesis authors' files submitted through the University Graduate School.

A Thesis Submitted in Partial Fulfillment of the Requirements  
for the Degree of Master of Science Program in Hazardous Substance and  
Environmental Management  
(Interdisciplinary Program)  
Graduate School  
Chulalongkorn University  
Academic Year 2016  
Copyright of Chulalongkorn University

การสังเคราะห์อนุภาคนาโนเหล็กประจุศูนย์ จากน้ำเสียที่ปนเปื้อนลิแกนด์เพื่อการกำจัดสารหนู



วิทยานิพนธ์นี้เป็นส่วนหนึ่งของการศึกษาตามหลักสูตรปริญญาวิทยาศาสตรมหาบัณฑิต

สาขาวิชาการจัดการสารอันตรายและสิ่งแวดล้อม (สหสาขาวิชา)

บัณฑิตวิทยาลัย จุฬาลงกรณ์มหาวิทยาลัย

ปีการศึกษา 2559

ลิขสิทธิ์ของจุฬาลงกรณ์มหาวิทยาลัย

Thesis Title	Synthesis of Nanoscale Zerovalent Iron (nZVI) Derived from Lignin Containing Wastewater for Arsenic Removal
By	Mr. Phoomipat Jungcharoen
Field of Study	Hazardous Substance and Environmental Management
Thesis Advisor	Associate Professor Jin Anotai, Ph.D.
Thesis Co-Advisor	Assistant Professor Tanapon Phenrat, Ph.D.

---

Accepted by the Graduate School, Chulalongkorn University in Partial  
Fulfillment of the Requirements for the Master's Degree

..... Dean of the Graduate School  
(Associate Professor Sunait Chutintaranond, Ph.D.)

THESIS COMMITTEE

..... Chairman  
(Associate Professor Srilert Chotpantarat, Ph.D.)

..... Thesis Advisor  
(Associate Professor Jin Anotai, Ph.D.)

..... Thesis Co-Advisor  
(Assistant Professor Tanapon Phenrat, Ph.D.)

..... Examiner  
(Dao Suwansang Janjaroen, Ph.D.)

..... External Examiner  
(Assistant Professor Bunyarit Panyapinyopol, Ph.D.)

ภูมิภัทร จึงเจริญ : การสังเคราะห์อนุภาคนาโนเหล็กประจุศูนย์ จากน้ำเสียที่ปนเปื้อน  
 ลิกนินเพื่อการกำจัดสารหนู (Synthesis of Nanoscale Zerovalent Iron (nZVI)  
 Derived from Lignin Containing Wastewater for Arsenic Removal) อ.ที่ปรึกษา  
 วิทยานิพนธ์หลัก: รศ. ดร. จินต์ อโณทัย, อ.ที่ปรึกษาวิทยานิพนธ์ร่วม: ผศ. ดร. ธนพล  
 เพ็ญรัตน์, 81 หน้า.

อนุภาคนาโนเหล็กประจุศูนย์ (nZVI) มีบทบาทสำคัญในการฟื้นฟูสิ่งแวดล้อมรวมถึง  
 การกำจัดสารหนูจากน้ำบาดาลและน้ำดื่ม งานวิจัยนี้สังเคราะห์อนุภาคนาโนเหล็กประจุศูนย์ดัดแปร  
 เพื่อกำจัดสารหนูในน้ำดื่ม การตกตะกอนผลึกแบบบริดจ์ขึ้นภายใต้สภาวะต่างๆถูกใช้ในการผลิต  
 อนุภาคนาโนเหล็กประจุศูนย์ที่ไม่ดัดแปร (B-nZVI) และที่ดัดแปรด้วยลิกนินโดยใช้ 1 กรัม/ลิตร  
 สารละลายลิกนิน (L-nZVI) หรือน้ำเสียเชื้อและกระดาษ (P-nZVI) เป็นขั้วเสถียร สัดส่วนโมลาร์  
 ของเฟอร์รัสและโบโรไฮไดรด์ที่เหมาะสมที่สุดคือ 1:1 สำหรับการผลิต L-nZVI และ P-nZVI  
 เนื่องจากลิกนินถูกรวมเข้าไปในโครงสร้างของอนุภาคนาโนเหล็กประจุศูนย์มากที่สุด ผลการ  
 วิเคราะห์ TEM พบว่าขนาดอนุภาคของ B-nZVI, L-nZVI และ P-nZVI คือ  $52.72 \pm 17.58$ ,  
 $4.77 \pm 3.51$ , and  $2.04 \pm 1.09$  นาโนเมตรตามลำดับ พื้นที่ผิวจำเพาะของ P-nZVI (49.36 ตาราง  
 เมตรต่อกรัม) สูงกว่าของ L-nZVI (13.32 ตารางเมตรต่อกรัม) มาก ซึ่งน่าจะเป็นผลมาจากการที่มี  
 โพลีเมอร์อื่นร่วมอยู่ด้วยเช่น คาร์โบไฮเดรต แทนนิน กรดอินทรีย์ สารประกอบซัลเฟอร์ และเรซิน  
 ผลการศึกษาการกำจัดสารหนูพบว่า B-nZVI, L-nZVI และ P-nZVI ที่ 1 กรัมต่อลิตรสามารถ  
 กำจัดสารหนูทั้งหมดที่ 1 มิลลิกรัมต่อลิตรได้ร้อยละ 88.79, 88.66, และ 90.79 ตามลำดับในเวลา  
 5 นาที

สาขาวิชา การจัดการสารอันตรายและ  
 สิ่งแวดล้อม

ปีการศึกษา 2559

ลายมือชื่อนิติกร .....

ลายมือชื่อ อ.ที่ปรึกษาหลัก .....

ลายมือชื่อ อ.ที่ปรึกษาร่วม .....



## ACKNOWLEDGEMENTS

First of all, I would like to graciously thank my advisor Assoc. Prof. Jin Anotai and co-advisor Asst. Prof. Tanapon Phenrat for their support and assistance and the opportunities they have given to me during my master's degree research at King Mongkut's University of Technology Thonburi and Naresuan University. Their advice and encouragement empowered me to create and perform my research each step of the way.

I would like to give a special thanks to the International Postgraduate Program in Hazardous Substance and Environmental Management at the Center of Excellence on Hazardous Substance Management (HSM) of Chulalongkorn University. I am also appreciative of the 90th Anniversary of Chulalongkorn University Fund (Ratchadaphiseksomphot Endowment Fund Batch 35) for giving financial support for this research. Moreover, this research has performed at the Environmental Engineering Laboratory, of the Faculty of Engineering, at Naresuan University.

I also really appreciate my committee members, Assoc. Prof. Dr. Srilert Chontpantararat, Dr. Penradee Chanpiwat, Asst. Prof. Dr. Chantra Tongcumpou, Dr. Dao Suwansang Janjaroen, and Asst. Prof. Dr. Bunyarit Panyapinyopol, for their advice and time. Moreover, I would like to thank Ms. Akiko Uyeda for helping to improve my English skills.

I am also grateful to my friends for their support, particularly Ms. Warangluck Sonklin, Mrs. Witchaya Imkrajang, Ms. Nipawan Chuntakun, Mr. Somkiet Chaipun, Mrs. Prakaithip Kitikhun, Ms. Thanita Sutthatang, Ms. Vinita Khamin, Mr. Itsaraphong Kumloet, and Acting Sub Lt. Thitiporn Pladboon of Naresuan University.

Finally, I would like to thank my lovely family and all my friends at the three universities on my master's degree life: Naresuan University, King Mongkut's University of Technology Thonburi, and Chulalongkorn University.

## CONTENTS

	Page
THAI ABSTRACT .....	iv
ENGLISH ABSTRACT.....	v
ACKNOWLEDGEMENTS .....	vi
CONTENTS.....	vii
LIST OF TABLES .....	1
LIST OF FIGURES .....	2
CHAPTER I Introduction .....	4
1.1 General information.....	4
1.2 Hypotheses.....	6
1.3 Research objectives .....	6
1.4 Research scope.....	7
1.5 Research methodology.....	8
CHAPTER II Theories and literature review.....	10
2.1 Pulp and paper .....	10
2.2 Nanoscale zerovalent iron (nZVI) .....	11
2.2.1 Background .....	11
2.2.2 nZVI particle structure .....	12
2.2.3 Modified nZVI .....	13
2.2.4 Synthesis of nZVI.....	16
2.3 Mechanism of heavy metals by nZVI.....	19
2.4 Mechanisms of arsenic by nZVI.....	21
CHAPTER III Methodology .....	26
3.1 Apparatus.....	26
3.2 Synthesis of nZVI.....	27
3.2.1 Chemical reagents .....	27
3.2.2 Methods .....	27
3.3 General parameter measurements.....	28
3.3.1 Chemical reagents and materials.....	28

	Page
3.3.2 Methods .....	29
3.3.2.1 Before removing nZVI .....	29
3.3.2.2 After removing nZVI and then filtration .....	29
3.4 Arsenic removal .....	30
3.4.1 Chemical reagents and materials .....	30
3.4.2 Methods .....	30
3.5 Particle characterization.....	31
3.5.1 Chemical reagents and material .....	31
3.5.2 Methods .....	31
3.6 Measurement of hydrogen production.....	32
3.6.1 Chemical reagents and materials.....	32
3.6.2 Methods .....	32
CHAPTER IV RESULTS AND DISCUSSIONS .....	33
4.1 Synthesis of nZVI .....	33
4.1.1 Lignin-modified nZVI.....	33
4.1.1.1 Effect of molar ratio .....	33
4.1.1.2 Effect of mass ratio.....	35
4.1.2 pulp-modified nZVI (P-nZVI).....	37
4.1.3 non-modified nZVI (bare nZVI) .....	38
4.1.4 Comparison of various forms nZVI .....	38
4.2 Characterization of nZVI particles .....	41
4.2.1 Transmission electron microscopy (TEM).....	41
4.2.2 Scanning Electron Microscope (SEM).....	44
4.2.3 Energy Dispersive X-ray spectroscopy (EDX) .....	45
4.2.4 X-ray powder diffraction (XRD).....	47
4.2.5 Brunauer-Emmett-Teller (BET) .....	49
4.3 Arsenic removal by nZVI .....	50
4.3.1 Lignin-modified nZVI.....	50
4.3.1.1 Open system .....	50

	Page
4.3.1.2 Closed system.....	55
4.3.1.3 Comparison .....	57
4.3.2 Various forms of nZVI.....	59
4.3.2.1 Open system .....	59
4.3.2.2 Closed system.....	63
4.3.2.3 Comparison .....	65
CHAPTER V CONCLUSION AND RECOMMENDATIONS .....	67
5.1 Conclusion .....	67
5.2 Recommendations.....	67
REFERENCES .....	68
APPENDIX.....	72
Appendix A: Properties of nZVI .....	73
Appendix B: lignin removal by nZVI commercial and color removal.....	76
Appendix C: Calibration curve of lignin, iron, arsenic, and hydrogen production.....	78
VITA.....	81

## LIST OF TABLES

<b>Table 2.1</b> Reported modification methods for nZVI.....	15
<b>Table 2.2</b> Methods for the synthesis of nZVI.....	17
<b>Table 2.3</b> Standard redox potential ( $E^0$ ) in aqueous solution at 25°C .....	20
<b>Table 3.1</b> Characteristic pure lignin and pulp wastewater. ....	29
<b>Table 4.1</b> Particle sizes of various forms of nZVI and mass ratios of $Fe^{2+}$ to $BH_4^-$ on lignin for L-nZVI. ....	41
<b>Table 4.2</b> Effect of L-nZVI and P-nZVI on Atomic weight percent by EDX. ....	45
<b>Table 4.3</b> The pseudo first-order rate constant of total arsenic removal and half-life in various forms of nZVI. ....	51

## LIST OF FIGURES

<b>Figure 1.1</b> Overview of the steps for the synthesis of L-nZVI, and P-nZVI. ....	8
<b>Figure 1.2</b> Experimental scenarios.....	9
<b>Figure 2.1</b> Nanoscale zerovalent iron particle for in situ groundwater remediation...	12
<b>Figure 2.2</b> Core-shell structure of nZVI depicting various mechanisms for the removal of metals and chlorinated compounds. (Adapted from Li et al., 2006.) .....	13
<b>Figure 3.1</b> Synthesis of nZVI .....	28
<b>Figure 4.1</b> Effect of various molar ratios of $\text{Fe}^{2+}$ to $\text{BH}_4^-$ for L-nZVI on (a) removal efficiency and (b) suspended solid.....	34
<b>Figure 4.2</b> Effect of various mass ratios of $\text{Fe}^{2+}$ to $\text{BH}_4^-$ for L-nZVI on (a) removal efficiency (b) suspended solid and (c) dissolved iron.....	36
<b>Figure 4.3</b> Effect of P-nZVI on removal efficiency.....	37
<b>Figure 4.4</b> Effect of various forms of nZVI on (a) removal efficiency, (b) suspended solid and (c) dissolved iron. ....	39
<b>Figure 4.5</b> Conceptual model for various forms of nZVI (a) bare nZVI, (b) L-nZVI, (c) P-nZVI, and (d) L-nZVI commercial. ....	40
<b>Figure 4.6</b> Representative TEM images of (a) bare nZVI, (b) L0.01:0.01, (c) L0.02:0.02, (d) L0.04:0.04, (e) L0.08:0.08, and (f) P0.01:0.01 at 135 kx magnification with scale bar 50 nm. ....	43
<b>Figure 4.7</b> SEM images of (a) L0.01:0.01, (b) L0.02:0.02, (c) L0.04:0.04, (d) L0.08:0.08, and (e) P0.01:0.01 at 1000X magnification. ....	44
<b>Figure 4.8</b> EDX analyses of (a) L0.01:0.01, (b) L0.02:0.02, (c) L0.04:0.04, (d) L0.08:0.08, and (e) P0.01:0.01. ....	46
<b>Figure 4.9</b> XRD patterns of (a) L0.01:0.01, (b) L0.02:0.02, (c) L0.04:0.04, (d) L0.08:0.08, and (e) P0.01:0.01. ....	48

<b>Figure 4.10</b> BET surface area of (a) L0.01:0.01, (b) L0.02:0.02, (c) L0.04:0.04, (d) L0.08:0.08, (e) P0.01:0.01. ....	49
<b>Figure 4.11</b> Effect of the various mass ratios of $\text{Fe}^{2+}$ to $\text{BH}_4^-$ for L-nZVI on (a) total arsenic removal, (b) pH, and (c) ORP within 2.5, 5, 15, 30, and 60 minutes.....	53
<b>Figure 4.12</b> ORP-pH diagram for the As-Fe- $\text{H}_2\text{O}$ in various forms of nZVI within..	54
<b>Figure 4.13</b> Effect of the various mass ratios of $\text{Fe}^{2+}$ to $\text{BH}_4^-$ for L-nZVI on (a) total and dissolved arsenic removal, (b) non-dissolved arsenic, (c) pH, and (d) ORP at 60 minutes.....	56
<b>Figure 4.14</b> Effect of various forms of nZVI on hydrogen production.....	57
<b>Figure 4.15</b> Comparison between open and closed system of the various mass ratios of $\text{Fe}^{2+}$ to $\text{BH}_4^-$ for L-nZVI on (a) total arsenic removal, (b) pH, and (c) ORP at 60 minutes.....	58
<b>Figure 4.16</b> Effect of the various forms of nZVI on (a) total arsenic removal, (b) pH, and (c) ORP within 2.5, 5, 15, 30, and 60 minutes. ....	61
<b>Figure 4.17</b> Conceptual model for total arsenic removal by various forms of nZVI (a) L-nZVI, (b) P-nZVI, and (c) bare nZVI. ....	62
<b>Figure 4.18</b> Effect of the various forms of nZVI on (a) total and dissolved arsenic removal, (b) non-dissolved arsenic, (c) pH, and (d) ORP at 60 minutes. ....	64
<b>Figure 4.19</b> Comparison between open and closed system of the various forms of nZVI on (a) total arsenic removal, (b) pH, and (c) ORP at 60 minutes. ....	66

## CHAPTER I

### Introduction

#### 1.1 General information

Nanomaterials are one of the significant technologies now widely used in industrial processes and for environmental remediation. Nano zerovalent iron (nZVI), in particular, have recently been identified as an advantageous agent for in situ remediation of some specific contaminants, such as chlorinated hydrocarbon and metallic elements (Grieger et al., 2010). Groundwater contamination is a significant global issue. Heavy metal (Ponder et al., 2000); (Kanel. et al., 2005) and chlorinated compounds (Lien & Zhang, 1999; Liu & Lowry, 2006) are found in groundwater and underground aquifers. However, the colloidal chemistry of bare nZVI allows it to adhere to soil surface and agglomerate, which declines the mobility and reactivity of nZVI (He & Zhao, 2005 ). Alternatively, nanoparticles can enhance stabilization with various surface coating agents such as carboxyl methyl cellulose and cellulose acetate (Wu & Ritchie, 2006). Thereby, this study was investigated that lignin has similar functional groups of these surface coating agents, and also treatment of pulp wastewater owing to a lot of lignin in pulp wastewater. Not only treatment of pulp in wastewater by reductive precipitation but also obtained lignin-modified nZVI.

Arsenic (As) in groundwater is naturally occurring and is considered to be one of the most environmentally hazardous substances owing to its toxicity with chronic exposure (Ravenscroft et al., 2009). In addition to the normal presence of arsenic, coming from natural processes such as volcanic emissions, weathering reactions, and biological activities, it also results from anthropogenic activities such as pesticide use, mining activities and the burning of fossil fuels (Smedley & Kinniburgh, 2002). The arsenic contamination levels in groundwater have been measured in Ron Phibun District, Thailand, Taiwan, Bangladesh, and West Bengal (Anawar et al., 2002; Ng et al., 2003). The reported situations had serious environmental impacts. The recommended maximum arsenic level in potable groundwater is 0.01 mg/L, according to the World Health Organization (WHO, 1993). Arsenite, As(III), which has a higher mobility and toxicity than arsenate, is the focus of this research. The traditional methods

for removing arsenic from drinking water are reverse osmosis, chemical precipitation, microbial transformation, and adsorption (Kanel. et al., 2005). A study by (Chiu & Hering, 2000) illustrates that As(III) removal by these traditional water treatments is ineffective. The current practice includes the rapid removal of As(III) and As(V) from the subsurface environment by using zerovalent iron (ZVI) (Farrell et al., 2001; Lackovic et al., 2000; Mulder et al., 2011; NevarezL et al., 2011; Su & Puls, 2001; Yaich et al., 2012).

Pulp and paper production is a large industry that is significant to the Thai economy. The quantity of pulp and paper produced and consumed is increasing each year. Wastewater from the pulp and paper manufacturing process is highly polluted (USEPA,1998), and untreated wastewater contains high levels of lignin and its derivatives, tannins, sulphur compounds, and chlorinated compounds, which lead to high chemical oxygen demand (COD) and biological oxygen demand (BOD). The wastewater has a dark brown color, which is caused by polymerization between the lignin and tannin during the paper production process (Kalyani et al., 2009). To mitigate the environmental pollution caused by this industrial wastewater, it is necessary to treat it to achieve the regulatory effluent standards for effluent discharge into rivers. The effluent standards for COD and proposed color in manufacturing are less than 400 mg/L and 300 ADMI, respectively (Ministry of Natural Resources and Environment, Thailand, 2016).

Particular methods have been used for this purpose, including chemical treatments, physical processes, and biological methods, and different associations of these (Gurses et al., 2004). Several methods for eliminating color in pulp and paper manufacturing effluents, including chemical and physical processes, have been widely studied. These processes have included modified bleaching sequences, such as peroxide addition during extraction, ion-exchange chromatography, and soil ultrafiltration (Li et al., 2008). The drawback of the biological methods is a BOD:COD ratio (biodegradability index) of less than 0.02, which is quite low because the lignin contributes approximately 0-20mg/L of the BOD and a 750-780mg/L COD value in the wastewater (Kindsigo & Kallas, 2006). Apart from the biological methods, Kumar et al. (2011) demonstrated the wet air oxidation process can decrease COD, BOD and color in pulp and paper industrial waste. However, this method requires high energy,

pressure and costing equipment, makes this method uneconomical. Chemical precipitation uses ferrous sulphate, alum, ferric chloride and lime to treat wastewater. The disadvantages of this method are that it generates solid sludge and dewatering. Consequently, due to the various disadvantages inherent in these prior approaches, an effective treatment of pulp and paper wastewater is still being developed.

Currently, one alternative for the treatment of paper and pulp wastewater is reductive precipitation, which uses  $\text{Na}_2\text{S}$  for the removal of metals, including Hg, As, and Cu. Reductive precipitation can also be done by sodium borohydride in the presence of  $\text{Fe}_2\text{SO}_4$ , resulting in  $\text{Fe}^0$ , which can remove lignin from water. While other coagulation processes yield solid sludge only, the reductive precipitation process yields valuable by-products, including lignin-modified  $\text{Fe}^0$  nanoparticles, which may be useful for environmental restoration. For these reasons, the proposed project evaluated the feasibility of using the reductive precipitation of iron to treat pulp and paper wastewater, with the dual objectives of eliminating lignin, COD, and color (ADMI) and producing surface modified nZVI as a by-product. The potential for utilizing nZVI for remediation of Arsenic in drinking water was then evaluated.

## 1.2 Hypotheses

1.2.1 Lignin coating can improve nZVI properties both pure lignin and lignin in pulp and paper wastewater.

1.2.2 Lignin-modified nZVI could effectively remove arsenic in water.

## 1.3 Research objectives

1.3.1 To investigate the possibility of using reductive precipitation to treat lignin contaminated wastewater and to produce surface modified nZVI.

1.3.2 To characterize the physicochemical properties of surface modified nZVI as a result of the treatment of pulp and paper wastewater under various conditions.

1.3.3 To study the efficiency of removing arsenic by lignin-modified nZVI.

1.3.4 To find the optimum condition for using reductive precipitation to treat pulp and paper wastewater and to obtain optimum surface modified nZVI as by-product for arsenic remediation.

#### 1.4 Research scope

Using pulp wastewater from Wang Sala plant of SCG Paper, in Kanchanaburi, Thailand, this study focuses on two problems: (1) the applicability of lignin-modified nZVI in the treatment of pulp wastewater and (2) arsenic removal by lignin-modified nZVI. Specific aspects of the study are as follows:

- 1.4.1 Using both alkali lignin and pulp wastewater for nZVI modification.
- 1.4.2 Using a laboratory-scale reactor under room conditions.
- 1.4.3 Studied and analyzed parameters include pH, oxidation reduction potential (ORP), DO, COD, color (ADMI), conductivity, temperature, dissolved iron, lignin, and arsenic.
- 1.4.4 Using TEM, SEM, EDX, XRD, and BET to characterize the synthetic nZVI.
- 1.4.5 Hydrogen production was determined by GC-TCD.



## 1.5 Research methodology

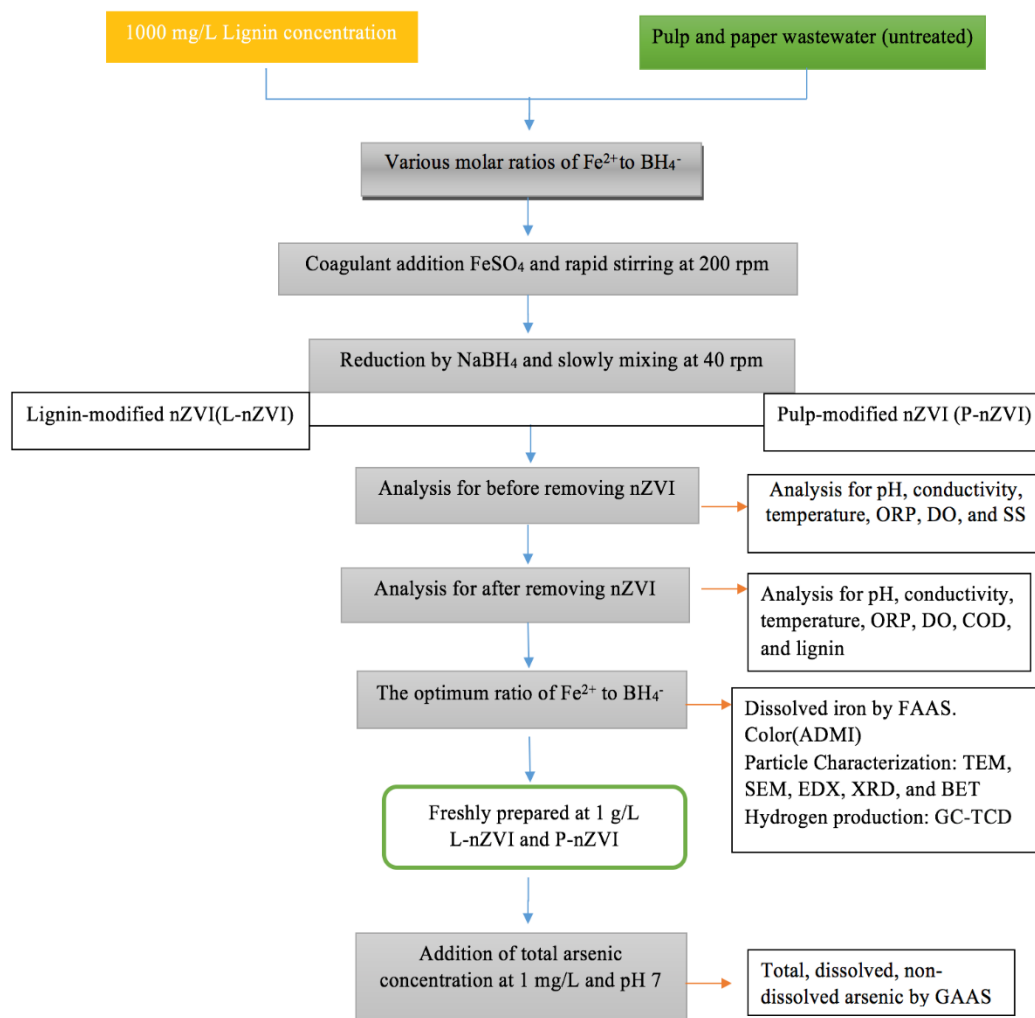


**Figure 1.1** Overview of the steps for the synthesis of L-nZVI, and P-nZVI.

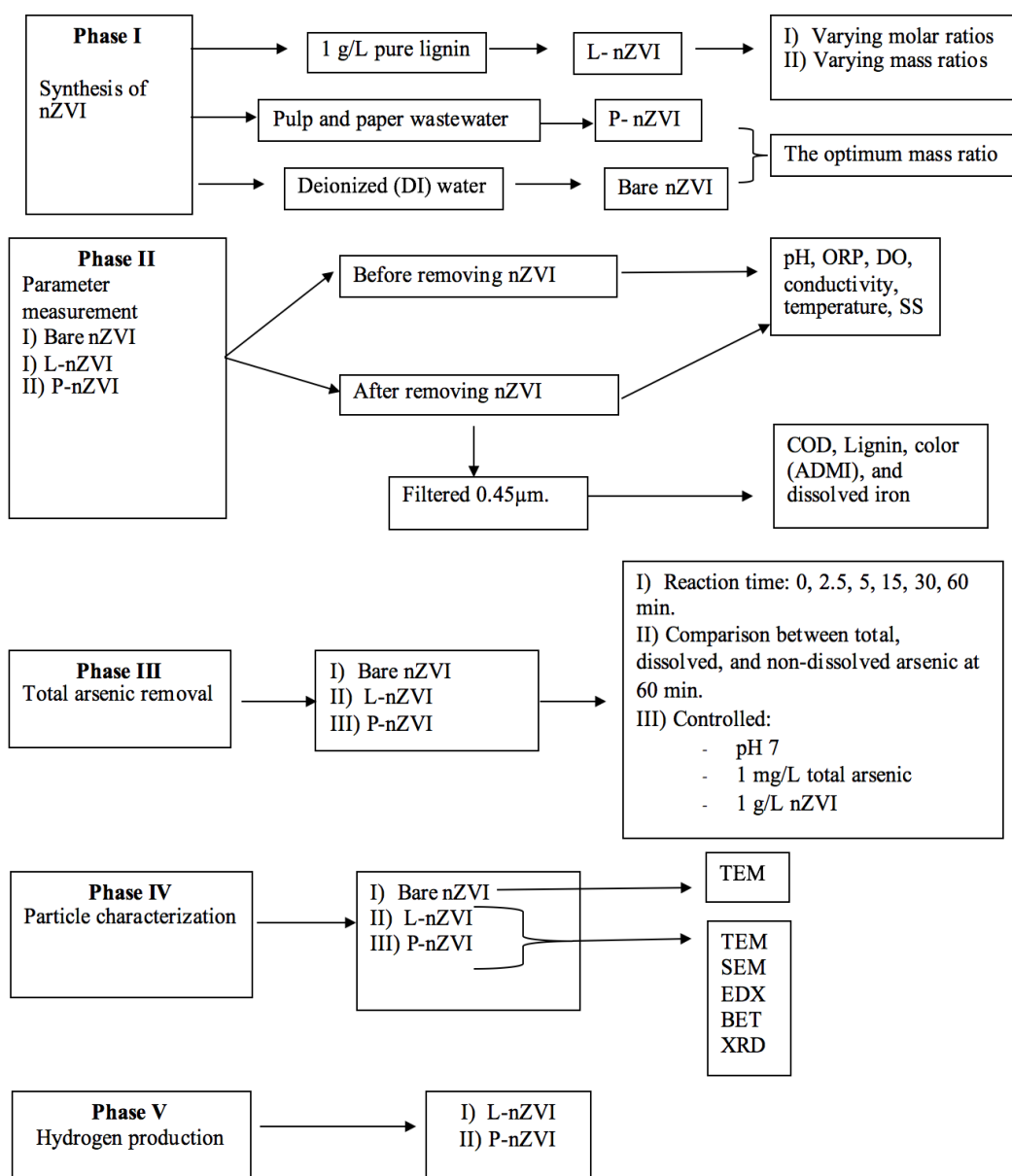


**Figure 1.2** Experimental scenarios.

## CHAPTER II

### Theories and literature review

#### 2.1 Pulp and paper

The water quality in natural occurring water sources, such as river and underground aquifers, is often quite low as a result of the discharge of untreated wastewater from industrial processes. This toxic situation has detrimental effects on human health and aquatic organisms. Cancer, in humans and animals, and mutations, in some cases, are known outcomes (Aghdam et al., 2016).

Black liquor from pulping processes in the paper making industry is an industrial wastewater pollutant, which contains a high amount of lignin. Lignin causes a strong color and high COD. Other pollutants in black liquor include aliphatic acid, phenolic compounds, organic acid, sulfur compounds, polysaccharides and resin (Kumar et al., 2011). About half of the composition of wood is cellulose. This is usually combined with lignin, and aromatic compounds with high molecular weight (Mosaferi et al., 2014). Lignin is composed of methoxyl groups, phenolic hydroxyl groups, and some terminal aldehyde groups in the side chains. The functional groups of lignin are aliphatic and aromatic hydroxyl groups, ether and ether linkages. In addition, these functional groups increase the reactivity of lignin. The lignin compounds occur in industrial wastes in massive amounts. Lignin contains three different structures depending on the position of methoxylation with hydroxycinnamyl alcohol monomers, including *p*-coumaryl, coniferyl, and sinapyl monolignols (Hambardzumyana et al., 2015). The covalent interactions of cellulose and lignin are electrostatic interactions composed of hydrogen bonds formed by carbonyl and methoxyl groups, alcoholic and phenolic hydroxyl and weaker van der Waals interactions of cell wall polymer designed that Fenton's reagent enhance lignin dispersion on cellulose nanocrystals.

Lignin sulfonate is one of the by-products from the pulping and papermaking process and exists in large amounts in the wastewater (Nyman et al., 1986). It is water soluble and harmless, and as a by-product of a usually large scale industrial process, lignin sulfonate exists in large quantities and is very inexpensive (Pang et al., 2008). Its usefulness as a stabilizing agent for silver nanoparticles has been demonstrated by

Milczarek et al. (2013). In addition, Laumann et al. (2014) found that the mobility of polyacrylic acid coated nZVI was enhanced by a co-injection of lignin sulfonate at concentrations of more than or equal to 50 mg/L.

Various terminology has been used in previous publications, particularly lignin sulfonate and Kraft lignin. This latter term is usually stated as a synonym, with an extended definition as 'Kraft lignin with low sulfonate content'. In this study, Kraft lignin is the term that will be used consistently. Fe<sub>3</sub>O<sub>4</sub> magnetic nanoparticles were investigated for their ability to remove lignin by adsorption. Mostashari et al. (2013) observed that poly-eugenol, which has the same structure as Kraft lignin, can be used as a stabilizing agent of gold nanoparticles. They further saw that Kraft lignin is a dispersal agent for carbon nanotubes, and they also employed softwood lignosulfonate (SLS) to stabilize silver nanoparticles with the reaction occurring on particle sizes of 41 nm on average. Their study supports the fact that the same functional groups in Kraft lignin are able to stabilize metal nanoparticles. In addition to being a dispersing agent of carbon nanotubes and stabilizing silver nanoparticles, lignins also have the potential to be an antibacterial agent, an antioxidant (Garcia et al., 2010) and a plasticization agent (Bouajila et al., 2006). Furthermore, industrial lignins, consisting of Kraft lignin, acetylated lignin containing cellulose fiber and lignosulfates, have been developed for material coatings or nanocomposite films (Mulder et al., 2011; NevarezL et al., 2011; Yaich et al., 2012).

## 2.2 Nanoscale zerovalent iron (nZVI)

### 2.2.1 Background

Sweeney and Fischer (1972) first used zerovalent metals such as zinc (Zn) for the removal of chlorinated compounds from the environment. Subsequently Senzaki and Kumagai (1988) used iron powder to remove chlorinated compounds from wastewater and groundwater contamination, as did (Gillham and O'Hannesin, 1994; Baciocchi et al., 2003). Gillham and O'Hannesin, (1994) present evidence of the efficiency of zerovalent iron (ZVI) for the degradation of ethane and chlorinated ethane. Wang and Zhang (1997) studied millimeter and micron size metals for environmental decontamination, and also theorized that the synthesis of nZVI was significant for two

reasons. Firstly, the nZVI particles have an extensive surface area to weight ratio, which leads to a faster reactivity rate than micron scale ZVI, and secondly, nZVI particles are smaller than most porous media pore throats. The potential application of nanoscale zerovalent iron particles applied for in situ groundwater remediation is shown in **Figure 2.1**

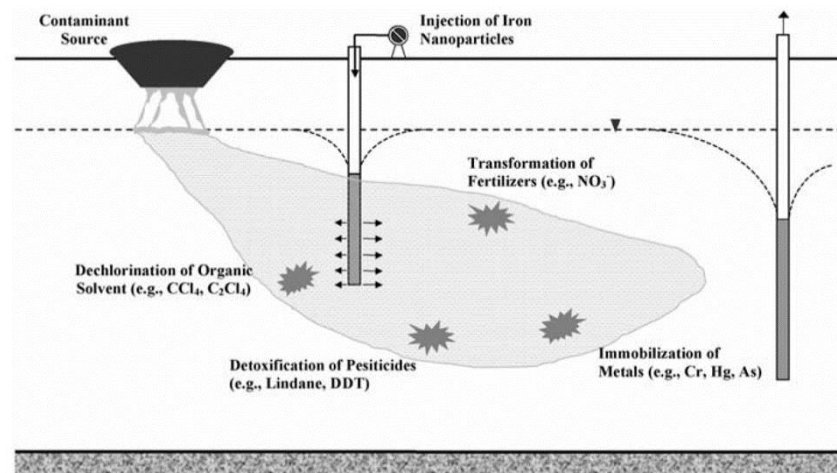


**Figure 2.1** Nanoscale zerovalent iron particle for in situ groundwater remediation. (Adapted from Zhang, 2003).

### 2.2.2 nZVI particle structure

Unamended nZVI particles are usually less than 100 nm in diameter, and react with oxygen and water to form an outer iron (hydr)oxide layer in aqueous solutions. Consequently, the nZVI particles have a core-shell shape (**Figure 2.2**)

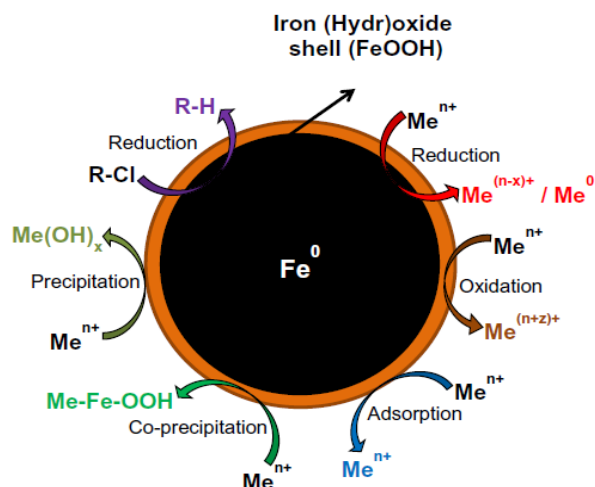


**Figure 2.2** Core-shell structure of nZVI depicting various mechanisms for the removal of metals and chlorinated compounds. (Adapted from Li et al., 2006).

The outer (hydr)oxide layer is able to act as a potential adsorbent for many contaminants such as metals. Zhang (2003) and Crane and Scott (2012) recommended four key properties of nZVI in in-situ remediation: (1) efficacy in treating highly reactive contaminants, (2) effective mobility through porous media, (3) reactive longevity, and (4) low toxicity. On the other hand, this process must have a reasonable cost and be able to compete with other processes for effectiveness and efficiency.

A potential drawback of applying nZVI particles is that they tend to aggregate into larger particles because of their high surface energy and internal magnetic interactions. Therefore, the aggregation affects both sufficient surface area and removal efficiency. The study of Wang et al. (2008) indicated that aggregated bare nanoscale particles are difficult to separate and recycle. However, the stability of nZVI particles can increase with different surface coating agents.

### 2.2.3 Modified nZVI

Normally, nanomaterials (NMs) can attach to the mineral surface, which might cause low mobility in groundwater aquifers. Nonetheless, nZVI is commonly used in site remediation, but information on the environmental outcomes and ultimate

destination and transport of the nZVI, is not yet sufficient. The factors affecting this situation include the synthesis of the nZVI method, contaminant concentration, aging nZVI, hydraulic properties of the aquifer, and geochemical properties (e.g., pH, DO, and ORP). Various conditions that may create agglomeration constituents of the nZVI concentration include size distribution and the presence of magnetic particles. A high concentration of nZVI particles might lead to agglomeration. (Phenrat et al., 2007) discovered that smaller particles with low ZVI concentrations can travel further than larger particles with high nZVI concentrations.

Different organic coatings currently available include polyelectrolytes, polymers, and emulsions that augment the mobility of iron nanoparticles in the subsurface and also decrease the reactivity. This is the focus of this research: lignin's presence in pulp and paper wastewater and its subsequent use as a polymer. Various coating agents, including polymer and polyelectrolytes, have been studied as supporting materials for nZVI:

1. Cellulose derivatives: CMC (He & Zhao, 2005 ), cellulose acetate (Wu & Ritchie, 2006)
2. Hydrophilic biopolymers such as starch, guar gum, alginate, and aspartame (Bezbaruah et al., 2009; Saleh et al., 2008; Tiraferri & Sethi, 2009).
3. Natural organic matter such as humic acid (Xie & Shang, 2005; Zhu et al., 2008).
4. Chitosan (Geng et al., 2009).
5. Polyelectrolytes such as polyacrylic acid, ion-exchange resins, and block copolymers (Kanel et al., 2007; Sirk et al., 2009).
6. Chelating agents: ethylenediaminetetraacetic acid (EDTA), nitriloacetic acid (NTA), and hydroxyethylenediaminetetraacetic acid (HEDTA) (Allabaksh et al., 2010).
7. Amphiphiles including various surfactants, which can be anionic, cationic, or non-ionic (Hydutsky et al., 2007; Kanel and Choi, 2007; Zhu

et al., 2008) and block copolymers (Saleh et al., 2005; Saleh et al., 2007; Saleh et al., 2008)

In addition, some successfully applied modification methods are presented in **Table 2.1**. All these supporting materials can assist in inhibiting the aggregation of nZVI particles by stabilization (Stefaniuk et al., 2016). The functional group structures of the supporting materials are similar to lignin. Hence, this project selected lignin to modify nZVI.

**Table 2. 1** Reported modification methods for nZVI

Modifying agent	Type of particle	The role of the modifying agent	Other
Copolymer (vinyl alcohol–vinyl acetate, itaconic acid) (PV3A)	nZVI	To improve the surface properties, increase the stability and reduce the particle size (<10 nm)	98% removal of TCE after 3 hr.
Poly(methylmethacrylate) in anisole (PMMA)/anisole	nZVI	To retard oxidation of nZVI and reduce agglomeration	A coating of PMMA/anisole reduces the efficiency of removal of dye in comparison to BnZVI
Bamboo	nZVI	To retards oxidation of nZVI, reduce aggregation, ease recovery after the application	79.6% removal of methylene blue dye in aqueous solution
Rice hull derived biochar	nZVI	To increase the surface area	99.4% removal of TCE

Graphene	nZVI	To use of a stable support	Efficient removal of phosphate from aqueous solutions
Chitosan fibers	nZVI	To immobilize nZVI using fibers with a large specific surface area	The material was effectively used in As(III) and As (V) uptake from aqueous systems

#### 2.2.4 Synthesis of nZVI

There are many possible ways to synthesize nZVI, which can be divided into physical and chemical methods. Physical methods include abrasion, grinding, and lithography. Chemical methods have evolved through the use of a reducing agent, such as sodium borohydride ( $\text{NaBH}_4$ ). A crucial benefit of this method is its simplicity but these methods need to be cautiously applied. Practical techniques for synthesizing nZVI are summarized in **Table 2.2** (Stefaniuk et al., 2016).

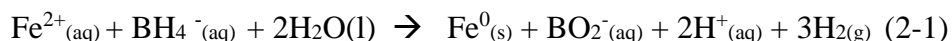


**Table 2.2** Methods for the synthesis of nZVI.

Method	Short description	Benefits	Drawbacks	Diameter (nm.)	Surface area [m <sup>2</sup> /g]
Lithography Grinding	Break down bulk iron materials	Inexpensive method	Limited control over particle size distribution and morphology	Not available (N.A.)	N.A.
Precision milling method	The rotary chamber with steel beads	Elimination of toxic reagents, short processing time, low energy consumption	N.A.	10–50	39.0
Chemical reduction	Reduction of the iron salts using reducing agent	Simple and easy to use in any laboratory	The use of toxic reducing agent	1–100	33.5

Carbothermal reduction	Fe <sup>2+</sup> are reduced to nZVI at elevated temperatures with the use of thermal energy in the presence of gaseous reducing agents	Spherical iron particles, cheap reducing agent –H <sub>2</sub> , CO <sub>2</sub> , CO	Not well known	20–150	130
Ultrasound method	Application of ultrasound waves and reducing agent	The creation of small nanoparticles	The use of toxic reducing agent	10	34.0–42.0
Electrochemical method	Reduction of the iron salt in the presence of the electrodes and electrical	Inexpensive method	Tendency to form nZVI clusters	1–20	25.4
Green synthesis	Biosynthesis of nanoparticles using plant extracts	Replacing toxic reducing agent	Irregular shape	20–120	5.8

Conventionally, nZVI is synthesized by using sodium borohydride (NaBH<sub>4</sub>) with either FeSO<sub>4</sub>·7H<sub>2</sub>O or FeCl<sub>3</sub>·6H<sub>2</sub>O. According to (Choi et al., 2008), NaBH<sub>4</sub> reacts with FeSO<sub>4</sub>·7H<sub>2</sub>O better than FeCl<sub>3</sub>·6H<sub>2</sub>O. For this reason, this research used FeSO<sub>4</sub>·7H<sub>2</sub>O with NaBH<sub>4</sub> for nZVI synthesis. The following describes the reaction (He & Zhao, 2005 ):



The most regularly used chemical method for synthesizing nZVI is chemical reduction, whereby the defining characteristic of the resultant product is a homogeneous structure that demonstrates high reactivity. In other words, lithography the synthesis of iron nanoparticles can be done using two approaches: top-down (, grinding, and precision milling method) and bottom-up (chemical reduction, carbothermal reduction, ultrasound, electrochemical method, and green synthesis). The advantages and disadvantages of each method are described in **Table 2.2**

Basavegowda and Lee (2013) believed that alternative eco-friendly syntheses of nanoparticles include fungi, micro-organisms, enzymes, plants or plant extracts as possible methods and are of interest for further research. In addition, these eco-friendly methods are less expensive, more rapid, and can more effectively produce different shapes (prims, spheres) with sizes from 1 to 100 nm.

### 2.3 Mechanism of heavy metals by nZVI.

nZVI material has a small particle size but large surface area, and high in-situ reactivity for soil, groundwater and sediment remediation, making it a useful and effective material for use in environmental engineering (Wang and Zhang, 1997; Lien et al., 1999; Ponder, et al., 2000).

According to (O'Carroll et al., 2013), the interactions between nZVI and various metals are as follows:

1. Reduction – Cr, As, Cu, U, Se, Co, Pd, Pt, Hg, Ag, Pb, Ni.
2. Adsorption – Cr, As, U, Pb, Ni, Se, Co, Cd, Zn, Ba.
3. Co-precipitation – Cr, As, Se, Ni.

4. Precipitation – Cu, Pb, Cd, Co, Zn.

5. Oxidation/reoxidation – As, Se, Pb, U.

Several metals are able to react with nZVI in more than one interaction. All these mechanisms with nZVI depend on the standard redox potential ( $E^0$ ) of the individual heavy metal as shown in **Table 2.3**

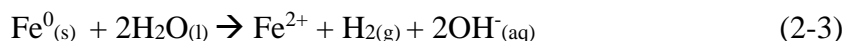
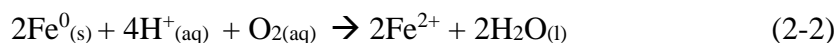
**Table 2.3** Standard redox potential ( $E^0$ ) in aqueous solution at 25°C  
(Bard et al., 1985; Wildeman and Verstraete, 2003)

Aqueous solution	Half reactions	$E^0$ (V)
Chromium (Cr)	$\text{CrO}_4^{2-} + 8\text{H}^+ + 3\text{e}^- \leftrightarrow \text{Cr}^{3+} + 4\text{H}_2\text{O}$	1.51
Chromium (Cr)	$\text{Cr}_2\text{O}_7^{2-} + 14\text{H}^+ + 6\text{e}^- \leftrightarrow 2\text{Cr}^{3+} + 7\text{H}_2\text{O}$	1.36
Platinum (Pt)	$\text{Pt}^{2+} + 2\text{e}^- \leftrightarrow \text{Pt}$	1.19
Palladium(P)	$\text{Pd}^{2+} + 2\text{e}^- \leftrightarrow \text{Pd}$	0.92
Mercury (Hg)	$\text{Hg}^{2+} + 2\text{e}^- \leftrightarrow \text{Hg}$	0.86
Silver (Ag)	$\text{Ag}^+ + \text{e}^- \leftrightarrow \text{Ag}$	0.80
Arsenic ( $\text{As}^{\text{V}}$ )	$\text{H}_3\text{AsO}_4 + 2\text{H}^+ + 2\text{e}^- \leftrightarrow \text{HAsO}_2 + 4\text{H}_2\text{O}$	0.56
Copper (Cu)	$\text{Cu}^{2+} + 2\text{e}^- \leftrightarrow \text{Cu}$	0.34
Uranium (U)	$\text{UO}_2^{2+} + 4\text{H}^+ + 2\text{e}^- \leftrightarrow \text{U}^{4+} + 2\text{H}_2\text{O}$	0.27
Arsenic ( $\text{As}^{\text{III}}$ )	$\text{H}_3\text{AsO}_3 + 3\text{H}^+ + 3\text{e}^- \leftrightarrow \text{As} + 3\text{H}_2\text{O}$	0.24
Copper ( $\text{Cu}^+$ )	$\text{Cu}^{2+} + \text{e}^- \leftrightarrow \text{Cu}^+$	0.16
Lead (Pb)	$\text{Pb}^{2+} + 2\text{e}^- \leftrightarrow \text{Pb}$	-0.13
Nickel (Ni)	$\text{Ni}^{2+} + 2\text{e}^- \leftrightarrow \text{Ni}$	-0.25
Cadmium (Cd)	$\text{Cd}^{2+} + 2\text{e}^- \leftrightarrow \text{Cd}$	-0.40
Iron (Fe)	$\text{Fe}^{2+} + 2\text{e}^- \leftrightarrow \text{Fe}$	-0.44
Zinc (Zn)	$\text{Zn}^{2+} + 2\text{e}^- \leftrightarrow \text{Zn}$	-0.76
Barium (Ba)	$\text{Ba}^{2+} + 2\text{e}^- \leftrightarrow \text{Ba}$	-2.92
1,2-Dichloroethane	$\text{ClH}_2\text{C}-\text{CH}_2\text{Cl} + 2\text{e}^- \leftrightarrow \text{H}_2\text{C}=\text{CH}_2 + 2\text{Cl}^-$	0.74
Carbon tetrachloride (CT)	$\text{CCl}_4 + \text{H}^+ + 2\text{e}^- \leftrightarrow \text{CHCl}_3 + \text{Cl}^-$	0.67
Tetrachloroethylene (PCE)	$\text{Cl}_2\text{C}=\text{CCl}_2 + \text{H}^+ + 2\text{e}^- \leftrightarrow \text{Cl}_2\text{C}=\text{CHCl} + \text{Cl}^-$	0.57
Trichloroethylene (TCE) Vin	$\text{Cl}_2\text{C}=\text{CHCl} + \text{H}^+ + 2\text{e}^- \leftrightarrow \text{Cl}_2\text{C}=\text{CH}_2 + \text{Cl}^-$	0.53
1,1-Dichloroethene (1,1- DCE)	$\text{Cl}_2\text{C}=\text{CH}_2 + \text{H}^+ + 2\text{e}^- \leftrightarrow \text{ClHC}=\text{CH}_2 + \text{Cl}^-$	0.42

The standard potential of iron is -0.44V, which is a sufficient, environmentally friendly, electron donor. For adsorption into the iron (hydr)oxide shell, the  $E^0$  of metals must be more negative than or similar to, that of  $\text{Fe}^0$  such as Zn and Cd. For reduction and precipitation, the  $E^0$  of metals must be more positive than  $\text{Fe}^0$  (i.e. As, Cr, Cu, U and Se). The metals with slightly more positive  $E^0$  than  $\text{Fe}^0$  are Ni and Pb.

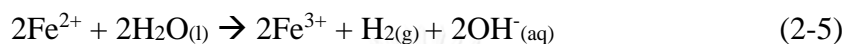
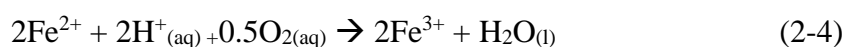
#### 2.4 Mechanisms of arsenic by nZVI.

After synthesizing the nZVI by the reducing the iron oxides ( $\text{Fe}^{2+}$ ) using sodium borohydride (as shown in **Equation 2-1**), the nZVI corrosion under the presence of oxygen is shown in **Equations 2-2 and 2-3**.



In further oxidative reactions as described in **Equations 2-4 and 2-5**.

(Crane and Scott, 2012).



Liang et al. (2014) suggested that the adsorption efficiency of nZVI can be raised by the FeOOH-shell. Under the limitation of oxygen, water and the corrosion reaction can give electron receptors, as shown in **Equations 2-6 and 2-7**.



Under the presence of oxygen, the corrosion of iron occurs, as shown in **Equation 2-8**.



In the aqueous phase,  $\text{Fe}^{2+}$  is produced at the surface first and immediately oxidized to  $\text{Fe}^{3+}$ , which further reacts with  $\text{OH}^-$  or  $\text{H}_2\text{O}$  to produce hydroxide or oxyhydroxide as shown in **Equations 2-9 and 2-10**.

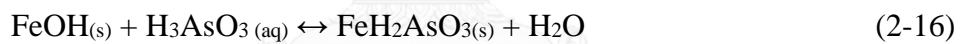
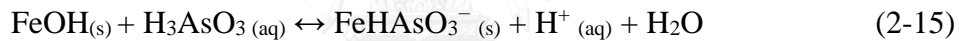
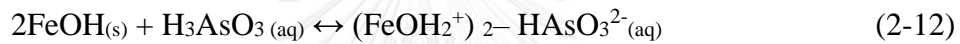
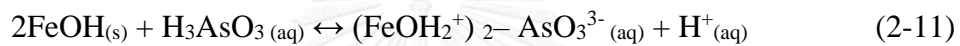


Further dehydration formate FeOOH.



The dominant species of arsenic existing in groundwater are inorganic arsenite, As(III) ( $\text{H}_3\text{AsO}_3$ ,  $\text{H}_2\text{AsO}_3^{1-}$ ,  $\text{HAsO}_3^{2-}$ ), and arsenate, As(V) ( $\text{H}_3\text{AsO}_4$ ,  $\text{H}_2\text{AsO}_4^{1-}$ ,  $\text{HAsO}_4^{2-}$ ) (Ferguson & Garvis, 1972; Manning et al., 2002). Arsenic removal by ZVI involves the formation of Fe(II) and Fe(III) corrosion products on the surface of iron owing to oxidation. The various corrosion products are a mixture of amorphous Fe (III) hydroxide or oxide, maghemite and/or magnetite, as mentioned before. These products are capable of As (III) and As (V) sorption by surface complexation (Tyrovola et al.,

2007). Zhu et al. (2008) investigated arsenite species, including  $\text{H}_3\text{AsO}_3$  and  $\text{H}_2\text{AsO}_3^-$ , in pH 9 and pH 9-12, respectively, which were dominant in solution. Moreover, at pH levels less than 9, arsenite adsorption was found to depend on the deprotonation of  $\text{H}_3\text{AsO}_3$ , but the electrostatic attraction or repulsion did not significantly affect the reaction since arsenite is predominantly a neutral molecule. When pH increased from 3 to 9, the deprotonation process of neutral arsenite molecules occurred, so the rate of adsorption increased. At pH levels of more than 9, a negative charge on the surface indicated electrostatic repulsion that repulsed arsenite anions, which lowered the adsorption performance. The arsenic removal mechanism is the inner-sphere and outer-sphere complexation between a ferric hydroxide surface and arsenite species, as suggested by Phenrat et al. (2007), and shown in **Equations 2-11 to 2-16**.



In addition, (Manning et al., 2002) presents implications of drinking water remediation. They found that As(III) was oxidized to As(V) during the  $\text{Fe}^0$  corrosion process under aerobic conditions. Interestingly, the conversion of As(III) led to low toxic levels of As(V), strongly adsorbed formation, and the co-precipitation of As(V) on iron oxide products. The products derived from the corrosion of  $\text{Fe}^0$ -40 and  $\text{Fe}^0$ -100 were a heterogeneous mixture of the iron oxides lepidocrocite and magnetite or maghemite. The oxidation of As(III) was initiated by the reaction of in-situ  $\text{Fe}^0$  corrosion, and iron oxides synthesis (hematite and maghemite). The application of  $\text{Fe}^0$  for As(III) and As(V) removal from water has been investigated, and the development of this technology further studied. It was found that  $\text{Fe}^0$  performed as a robust and economical material in an in-situ treatment of contaminants. The iron oxide sorbent formation and the possibility to oxidize As(III) to As(V) contribute  $\text{Fe}^0$  to react as a good choice for As removal water treatment.

Another possible pathway was described by (Kanel et al, 2005). Researcher performed arsenic (III/V) desorption and speciation experiments to find out the As(III)/(V) speciation after As(III) adsorption on nZVI. The desorption effect of As(III) oxidation to As(V) on nZVI corrosion was demonstrated. The As(V) recovery was highest at 20%, while the desorption of As(III) was 11% under 10 mg/L As(III) treatment. Moreover, it was found that As(III) can be removed; it took just a minute via adsorption on nZVI and this occurred over a wide range of pH levels and anion solutions. The reactive site on nZVI involves stable or metastable iron(II); mixed iron(II)/(III) or iron(III) oxide; and a hydroxide or oxyhydroxide corrosion product. As the nZVI corrodes over a longer period, more crystalline magnetite and lepidocrocite products will be detected during the process of As(III) adsorption. Hence, the reactive sites for As(III) adsorption on nZVI arises with time. Furthermore, As(III) locates close to the corroding NZVI surface is oxidized to As(V), it is adsorbed by an inner-sphere process that is similar to the As(III) on iron(III) oxide mechanism. This information confirmed that the NZVI removal process is involved in the oxidation of As(III) to As(V). (Joo et al., 2004; Voegelin & Hug, 2003) suggested that the formation of  $Fe^{2+}$  and  $H_2O_2$  were produced on the  $Fe^0$  surface in the form of the  $OH^\bullet$  radical as shown in the following equations:



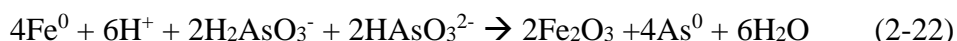
The As(III) oxidation reaction then proceeds as follows:



(Katsoyiannis et al., 2008) report that the following reactions take place on the  $Fe(0)$  surface: Fe(II) oxidation, green rusts formation,  $FeOOH/Fe_3O_4/Fe_2O_3$ -type layers (scales) passivating, and As(III) oxidation. The sorption of As to Fe(III) precipitates was explained as As(III) and As(V) reversible sorption to Fe(III)-dimers. The oxidant's nature plays an important role in reference to the pollutant type that can be oxidized. At a low pH, OH-radicals are the primary oxidant for As(III) and it has been expected that organic compounds should undergo oxidation at the same rate. At neutral pH, lower oxidant agents that were not deactivated by 2-propanol were generated. Meanwhile, this substance was able to efficiently oxidizes As(III), yet it could not oxidize some

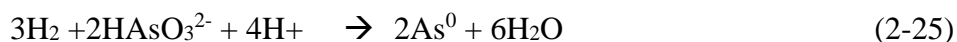
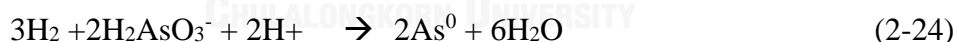
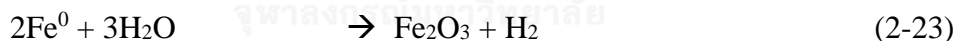
organic pollutants. Generally, organic pollutant degradation in the Fenton reaction usually performs efficiently at low pH conditions.

Tucek et al. (2017) suggested that possible pathways under anoxic conditions for the further reduction of As(III) species to As(0). They are described in **Equations 2-20 to 2-22**.



(Bang et al., 2005) studied that the arsenic removal by Fe (0) was induced As (III) electrochemical reduction to a little of As(0) and As(III) and As(V) were adsorbed on iron hydroxides formed on the surface of Fe(0) under anoxic conditions. These researchers found that when the solution is conducted in atmospheric air, the As(III) and As(V) removal rates were significant higher than under the anoxic condition. The adsorption on ferric hydroxides formed promptly through oxidation of Fe<sup>0</sup> by dissolved oxygen and caused immediate As(III) and As(V) removal.

Apart from that, Liu et al. 2005 suggested that atomic hydrogen can enhance the reactivity of an nZVI solution. Hydrogen may oxidize As<sup>3+</sup> to As<sup>0</sup> because of the redox potential and hydrogen that follows the oxidation of Fe<sup>0</sup> to Fe<sup>3+</sup> in water, as can be seen in **Equations 2-23 to 2-25**.



The structure of As (III) is either co-precipitated or adsorbed into the surface of nZVI (Kanel. et al., 2005; Ramos et al., 2009; Yan et al., 2010) demonstrated that 99% of arsenic(III) was removed from polluted water by 1g/L of nZVI. Mosaferi et al. (2014) successfully removed As(III) and As(V) by modifying nZVI to be either starch (S-nZVI) or carboxymethyl cellulose (C-nZVI). Their results indicate that S-nZVI has a higher reactivity than C-nZVI and bare nZVI. End products from nZVI reactions include iron hydroxides and iron oxide, which are environmentally friendly and offer insignificant health risks (Liu et al., 2006; Kumar et al., 2014)

For all the reasons discussed, and given the extent of research in the past, this research project can be considered to be both of interest and important in the scientific study area of environmental pollution remediation.



## CHAPTER III

### Methodology

This chapter describes the chemical agents and apparatus used for the synthesis of nZVI (bare-nZVI, lignin-modified nZVI, and pulp-modified nZVI), particle characterization, and the measurement of the parameters, total arsenic concentrations, and hydrogen production. According to O'Carroll et al. (2013), the parameters of nZVI in a field scale are pH, dissolve oxygen (DO), the oxidation reduction potential (ORP), suspended solids (SS), and dissolved iron. Therefore, pH, DO, the ORP, SS, conductivity, temperature, COD (close reflux), the lignin concentration, color (ADMI), dissolved iron, and the residual total arsenic concentration were the parameters measured in this study, and all experiments were performed at duplicates or triplicates.

#### 3.1 Apparatus

##### 3.1.1 Jar test equipment

##### 3.1.2 Peristaltic pump

##### 3.1.3 Silicone tube

##### 3.1.4 pH meter

##### 3.1.5 ORP meter

##### 3.1.6 Conductivity and temperature meter

##### 3.1.7 Small permanent magnet (450mT-500mT)

##### 3.1.8 UV-vis spectrophotometer

##### 3.1.9 ADMI spectrophotometer

##### 3.1.10 Ultrasonicator 500 Watts, 20 kHz

##### 3.1.11 Rotator mixer

##### 3.1.12 Microwave digester

##### 3.1.13 Flame atomic absorption spectrometry (FAAS)

##### 3.1.14 Graphite atomic absorption spectrometry (GAAS)

##### 3.1.15 Gas Chromatography-Thermal Conductivity Detector (GC-TCD)

## 3.2 Synthesis of nZVI

### 3.2.1 Chemical reagents

Ferrous sulfate heptahydrate ( $\text{FeSO}_4 \cdot 7\text{H}_2\text{O}$ ) and sodium borohydride ( $\text{NaBH}_4$ ) were purchased from Ajax, Australia. Alkali lignin was purchased from Aldrich Chemical Co. The sample of pulp and paper wastewater was received from SCG Paper. DI water was used from RO in the Naresuan University laboratory.

### 3.2.2 Methods

The chemicals used in this project to synthesize nZVI were  $\text{FeSO}_4$  in reaction with  $\text{NaBH}_4$ . Several researchers have demonstrated that the volume ratio of  $\text{FeSO}_4$  and  $\text{NaBH}_4$  might be equal, or 1:1, and the rate of dosing with  $\text{NaBH}_4$  should be slow. Moreover, Mosaferi et al. (2014); Jamei et al. (2014); and Huang et al. (2015) also suggested different molar ratios for these chemicals.

Hence, this project used various molar ratios of  $\text{FeSO}_4$  and  $\text{NaBH}_4$  levels (0.01:0.005, 0.01:0.01, 0.01:0.02, 0.01:0.04, 0.01:0.08) and various mass ratios of  $\text{FeSO}_4$  and  $\text{NaBH}_4$  levels (0.01:0.01, 0.02:0.02, 0.04:0.04, 0.08:0.08) with a dosing rate of 5 ml/min of  $\text{NaBH}_4$ , following the process in described by He and Zhao (2005).

Next, the jar tests, running several programs, were carried out. The jar tests included the following:

(a) adding  $\text{FeSO}_4$  at the desired concentration (100 mL) into a 1L beaker containing 500 mL of DI water (for unamended or bare nZVI), 500 mL of 1000mg/L lignin concentration (for lignin-modified nZVI), as well as 500 mL of pulp wastewater (for pulp-modified nZVI) for 30 seconds with rapid mixing at 200 rpm,

(b) adding  $\text{NaBH}_4$  at the desired concentration (100 mL) by using a peristaltic pump and fixed dosing rate of  $\text{NaBH}_4$  which is 5 ml/minute with slow mixing at 40 rpm for 20 minutes, as shown in **Figure 3.1** and

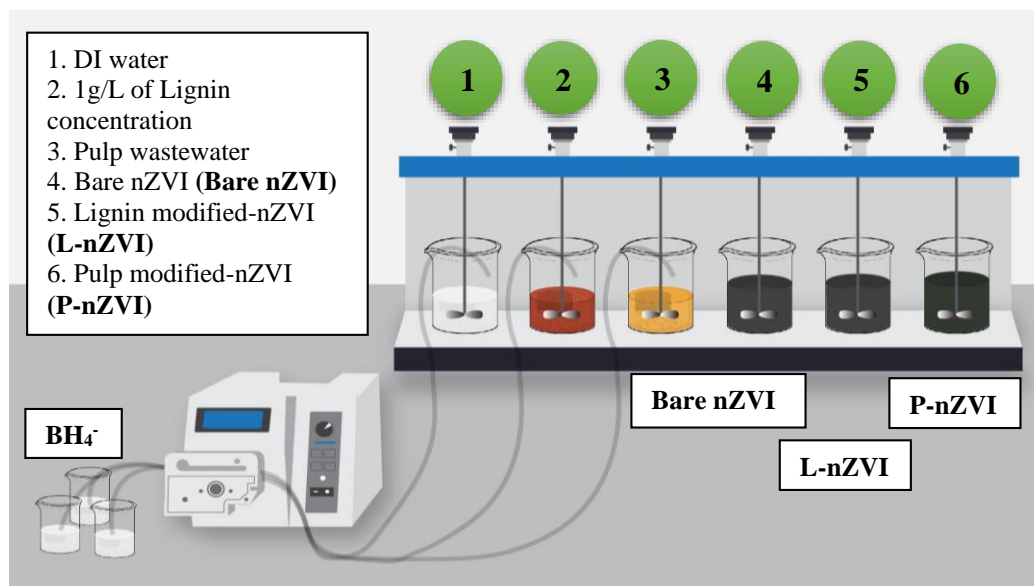


**Figure 3. 1** Systhesis of nZVI

(c) collecting the bare, lignin and pulp-modified nZVI in a beaker. Subsequently, a 50 mL beaker, with a diameter of 3 cm. and height of 3.4 cm. containing 25 mL of aqueous black suspension of iron nanoparticles was separated in a small permanent magnet (450mT-500mT) for 1 min, to separate iron nanoparticles and measure the pH, ORP, DO, conductivity, temperature, color, and COD. The bare, lignin and resulting pulp-modified nZVI and then be able to be applied for arsenic removal. The bare and pulp-modified nZVI were used the mass ratio which is the maximum lignin removal.

### 3.3 General parameter measurements

#### 3.3.1 Chemical reagents and materials

NaOH and HCl were used for pH adjustment in order to measure of the color using APHA 2120F, the ADMI Weighted-Ordinate Spectrophotometric Method. The other chemicals for analyzing COD were using by close reflux method. The COD was measured following the Standard Methods for the Examination of Water and Wastewater, 18<sup>th</sup> edited, 1992. Cellulose acetate (syringe filter 0.45 $\mu$ m), in a 5 mL syringe was filtrated in the lignin concentration, COD, color, and dissolve iron. The

HNO<sub>3</sub> for digestion and the chemical reagents and materials were purchased from Ajax, Australia. All chemicals were of laboratory grade.

### 3.3.2 Methods

#### 3.3.2.1 Before removing nZVI

After synthesizing each nZVI, the pH, ORP, DO, conductivity, temperature and suspended solid (SS) were measured both before and immediately after magnetic separation. All experiments were run in triplicate.

#### 3.3.2.2 After removing nZVI and then filtration

The samples of the separated iron nanoparticles were then filtered through a 0.45 µm syringe filter and examined to test the COD, color (ADMI), lignin concentration absorbed at 302 nm (adapted from Nevarez et al., 2011 and Mostashari et al., 2013), and the calibration curve of lignin is shown in **Figure C-1 and C-2**. Moreover, the dissolved iron concentration at various masses, for both FeSO<sub>4</sub> and NaBH<sub>4</sub>, using flame atomic absorption spectroscopy (FAAS). The calibration curve of iron concentration by FAAS is shown in **Figure C-4**.

This study investigates the increased lignin concentration that occurred with enhanced COD values. Therefore, the COD values of 1 g/L of pure lignin is close to COD of pulp wastewater, as can be seen in **Table 3.1** and **Figure C-3**. This is the reason why 1g/L of lignin was used for lignin-modified nZVI and pulp-modified nZVI. The properties of bare nZVI, L-nZVI, and P-nZVI were confirmed via triplicate experimental runs.

**Table 3.1** Characteristic pure lignin and pulp wastewater.

Sample	COD (mg/L)	Color (ADMI)	pH	Lignin concentration (mg/L) at 302 nm.	SS (mg/L)
1 g/L pure alkali lignin	1385.42	2850	8.43	999.88	0
Pulp and paper wastewater	1253.73	2130	6.09	196.09	111

### 3.4 Arsenic removal

#### 3.4.1 Chemical reagents and materials

The sodium arsenite solution (0.05 mol/L) was purchased from Merck Chemical Co. Arsenic standard solution was used for the analysis with a graphite atomic absorption spectrometer (GAAS). Cellulose acetate (syringe filter 0.45 $\mu$ m), a 5 mL syringe, and a 1 L polypropylene bottle were used. Moreover, a rotator mixer, Ultrasonicator (Sonics VC505), a 50 mL beaker, a 50 mL glass syringe, and silicone tube were used. The calibration curve of arsenic concentration by GAAS is shown in **Figure C-5**.

#### 3.4.2 Methods

Following that process, 1 g/L of each of the freshly prepared iron nanoparticles Bare-nZVI, L-nZVI, and P-nZVI was mixed with stock As solution at the total As concentration of 1 mg/L, which was prepared from a sodium arsenite solution of 0.05 mol/L at the initial of pH 7 in a 1L bottle containing 400 ml of arsenic. At the sonicated 2.50 minutes with 20 kHz and then the bottle was kept in the dark by covering it with aluminum foil and rotating it end over end in a rotator at 30 rpm for 60 minutes. At the 5 minutes, 15 minutes, 30 minutes and 60 minutes marks, samples were taken from the bottle. Furthermore, pH and ORP were measured for each sample. In this study was taken the sample at many times including 2.5, 5, 15, 30, 60 minutes, following the process in described (Mosaferi et al., 2014). It can be explained oxygen containing or open system. In addition, in this study was taken the sample just one time only at 60 minutes. It can be explained limited oxygen or close system.

Efficiency of total, dissolve, and non-dissolved arsenic removal were performed by bare nZVI, L-nZVI, and P-nZVI at 60 minutes. The residual arsenic concentration was identified by using GAAS. All experiments were at minimum duplicated. Moreover, the pH and ORP activity were observed the reactivity of these nZVI particles.

### 3.5 Particle characterization

#### 3.5.1 Chemical reagents and material

Methanol for dilution of bare nZVI, L-nZVI, and P-nZVI.

#### 3.5.2 Methods

To prepare the modified nZVI particles, the particles were dried in a vacuum overnight. The surface morphologies of the nanoparticles were characterized using a scanning electron microscope with energy dispersive X-ray spectroscopy (SEM-EDX), X-ray diffraction (XRD), and Brunauer-Emmett-Teller (BET).

3.5.2.1 A Philips Tecnai 12 transmission electron microscope (TEM), operated at 120kV, was used in this research. The nanoparticle samples, Bare-nZVI, L-nZVI, and P-nZVI, were prepared by a droplet of 1 mL of the nZVI sample and diluted nZVI containing 3 mL of methanol. After that, the samples were sonicated for 30 minute and put on 300-mesh carbon film with a copper grid to dry for 24 hours.

3.5.2.2 A scanning electron microscope with energy dispersive X-ray spectroscopy (SEM-EDX) was revealed structure and atomic weight on L-nZVI and P-nZVI.

3.5.2.3 X-ray diffraction (XRD) was conducted with a Philips analytical on L-nZVI and P-nZVI. The XRD method can perform crystal structure and composition analysis. In this study, 2theta was scanned from 10° to 80°, and scanning speed was 0.077278°/s at a tube voltage of 40 kV and current of 40 mA. The target type was copper, which has a wavelength of 0.1541 nm.

3.5.2.4 Brunauer- Emmett-Teller (BET) was performed specific surface area on L-nZVI and P-nZVI.

### 3.6 Measurement of hydrogen production

#### 3.6.1 Chemical reagents and materials

37 % HCl, a 60 mL glass vial, and Gas syringe volume was 500  $\mu\text{L}$  and 1000  $\mu\text{L}$  were performed for hydrogen production that was determined by a gas chromatograph equipped with a thermal conductivity detector (GC-TCD).

#### 3.6.2 Methods

The  $\text{Fe}^0$  content in the particles of the fresh nZVI sample were determined by particle digestion in concentrated HCl (Liu et al., 2005; Liu and Lowry, 2006; Garcia et al., 2016). 5 mL of 10 M HCl was injected to the 0.1 g nanoparticle samples in 60 mL glass vials. Therefore, hydrogen productions of various mass ratios of  $\text{Fe}^{2+}$  to  $\text{BH}_4^-$  for L-nZVI and P-nZVI at optimum condition were created by the reaction both nZVI ( $\text{Fe}^0$ ) and HCl can produce hydrogen gas. There is a 1:1 molar ratio between  $\text{Fe}^0$  and hydrogen as indicated in **Equation 3-1**. The reactor was capped and shaken for 30 minutes. After that, the resulting  $\text{H}_2$  was measured by a gas chromatograph (Model 2014AFT, Shimadzu) equipped with a thermal conductivity detector (GC-TCD) and a molecular sieve-13x column. Helium was used as the carrier gas with a total flow rate of 30 mL/min. The temperatures of the column and TCD were 42 and 120°C, respectively. The calibration curve of hydrogen (mole) produced by GC-TCD is shown in **Figure C-6**.



$$\frac{\text{mol hydrogen}}{\text{g nZVI}} = \frac{\text{mol hydrogen} * \text{volume of headspace}}{\text{g nZVI} * \text{volume of injection}} \quad (3-2)$$

## CHAPTER IV

### RESULTS AND DISCUSSIONS

#### 4.1 Synthesis of nZVI

In this part, various molar and mass ratios of  $\text{Fe}^{2+}$  to  $\text{BH}_4^-$  for 1 g/L lignin concentration in order to find the optimum ratio for synthesis of L-nZVI and various forms of nZVI including bare nZVI, L-nZVI, and P-nZVI were studied by using these parameters composed of pH, ORP, DO, temperature, conductivity, suspended solid, COD, lignin concentration, color (ADMI) and dissolved iron. **Table A-1** illustrates the properties of nZVI were pH, ORP, DO, temperature, and conductivity.

##### 4.1.1 Lignin-modified nZVI

###### 4.1.1.1 Effect of molar ratio

**Figure 4.1** demonstrates effect of various molar ratios of  $\text{Fe}^{2+}$  to  $\text{BH}_4^-$  for L-nZVI on (a) removal efficiency and (b) suspended solid. The various molar ratios of  $\text{Fe}^{2+}$  to  $\text{BH}_4^-$  for lignin-modified nZVI were not effective due to lower COD, lignin, and color removal as shown in **Figure 4.1 (a)** including L0.01:0.02, 0.01:0.04, and 0.01:0.08 because of increasing  $\text{BH}_4^-$  that was reducing agent and as seen color in **Figure B-2**. According to Standard methods for the examination of water and wastewater (Tannin and lignin 135, number 5550B, colorimetric method) suggested that 2 mg ferrous iron /L can produce a color equivalent to 1 mg tannic acid/ L. Hence, this reason might be affected by increasing lignin and color. Therefore, the optimum molar ratio of  $\text{Fe}^{2+}$  to  $\text{BH}_4^-$  for L-nZVI was 1:1 as shown in **Equation 2-1**.

**Figure 4.1 (b)** demonstrates effect of various molar ratios of  $\text{Fe}^{2+}$  to  $\text{BH}_4^-$  for L-nZVI on suspended solid. Suspended solid in the system is iron, iron oxide, and lignin. However, almost various molar ratios of  $\text{Fe}^{2+}$  to  $\text{BH}_4^-$  on suspended solid that was quite similar owing to use the same mole of iron.

At low ratio, pH is acidic because  $\text{FeSO}_4$  is acidic. However, when increasing  $\text{BH}_4^-$  concentrations were affected on more form  $\text{Fe}^0$  then the corrosion of  $\text{Fe}^0$  buffers

the pH system to be around 9- 10 which is typical for this  $\text{Fe}^0$  water system as shown in **Table A-1** and related on **Equation 2-2** and **2-3**.

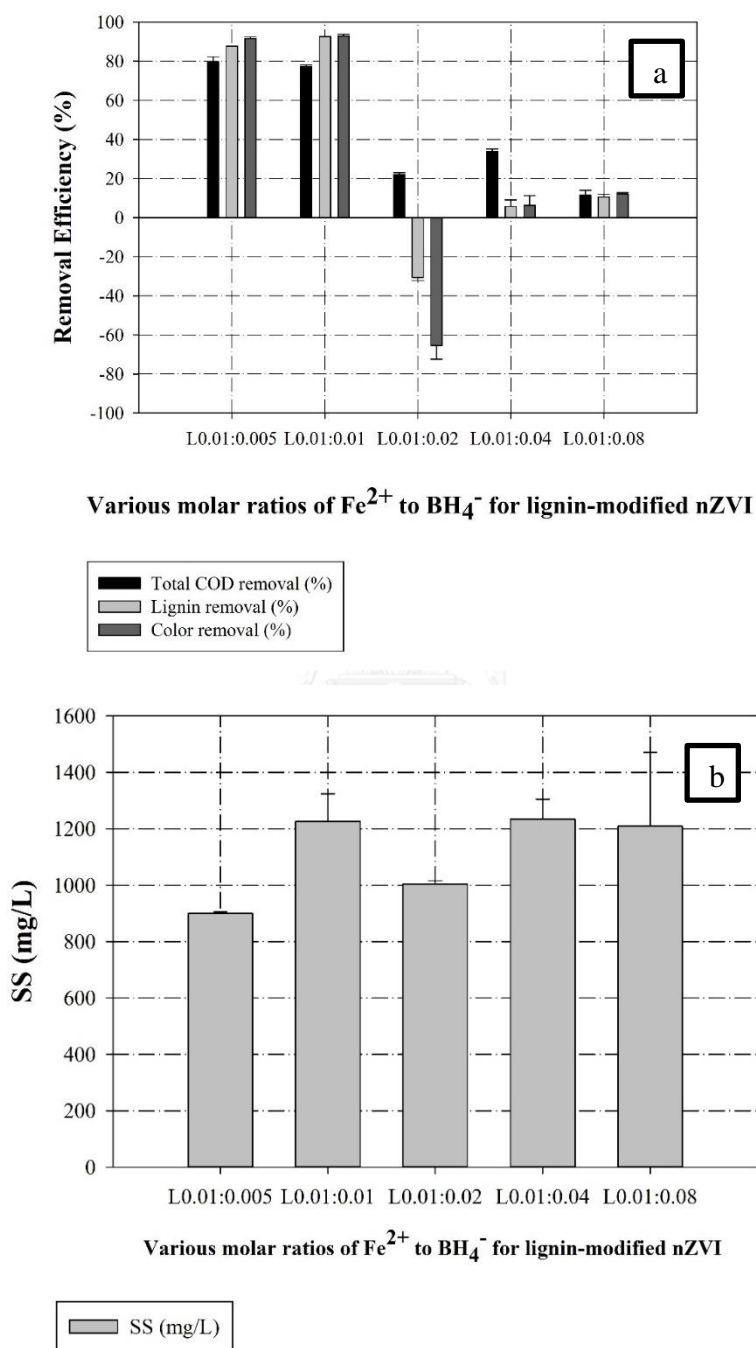


**Figure 4.1** Effect of various molar ratios of  $\text{Fe}^{2+}$  to  $\text{BH}_4^-$  for L-nZVI on (a) removal efficiency and (b) suspended solid.

#### 4.1.1.2 Effect of mass ratio

**Figure 4.2 (a)** illustrates the efficiency of total COD removal was decreased and provided 77.37, 71.84, 57.89, and 31.05% because of increasing mass ratios of  $\text{Fe}^{2+}$  to  $\text{BH}_4^-$ .

The efficiency of decolorization that provides 92.98%, 92.51%, 92.09%, and 91.62% by slight decreasing the efficiency with increasing the mass ratios of  $\text{Fe}^{2+}$  to  $\text{BH}_4^-$ . The efficiency of lignin removal provides 92.40%, 91.52%, 90.72%, and 90.29% by decreasing the efficiency with increasing the mass ratios of  $\text{Fe}^{2+}$  to  $\text{BH}_4^-$  within 20 minutes. The results were effective decolorization and lignin removal because nZVI particles have high surface area that means highly absorbed lignin on the surface. All the results of total COD, decolorization, and lignin removal were related by increasing the mass ratios of  $\text{Fe}^{2+}$  to  $\text{BH}_4^-$ .

**Figure 4.2 (b)** demonstrates increasing suspended solid with increasing mass ratios of  $\text{Fe}^{2+}$  to  $\text{BH}_4^-$ . Therefore, basically different ratio may just result in different amount of NZVI which subsequently results in difference in lignin COD or color removal efficiency.

**Figure 4.2 (c)** demonstrates effect of various mass ratios of  $\text{Fe}^{2+}$  to  $\text{BH}_4^-$  for L-nZVI on dissolved iron. Dissolved iron concentrations were 7.09, 23.24, 1942.56, and 3873.06 mg/L. Dissolved iron concentrations were increased because of increasing  $\text{FeSO}_4$  in solution so these concentrations have more leftover  $\text{Fe}^{2+}$ . Moreover, dissolved iron could explain stability of nZVI. Generally, the stability of nZVI particles could be the various forms of iron oxide. Therefore, L0.01:0.01 may be stable than each the various mass ratios because of low dissolved iron. According to these resulting from lignin and color removal, the optimum mass ratio of  $\text{Fe}^{2+}$  to  $\text{BH}_4^-$  was 0.01: 0.01 by the highest lignin and color removal. Therefore, this research was used the optimum ratio for bare nZVI and pulp-modified nZVI and applied on arsenic removal.

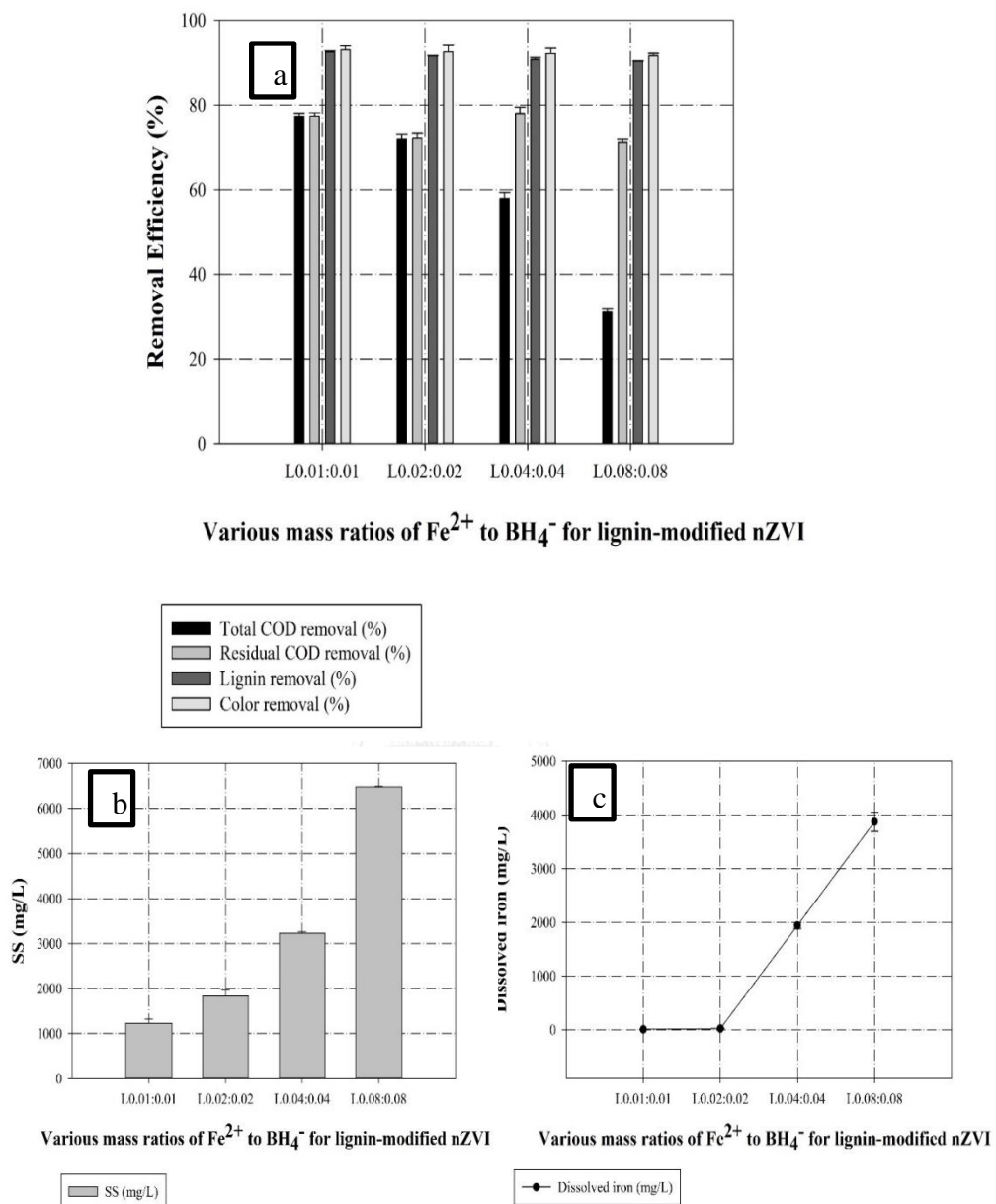


**Figure 4.2** Effect of various mass ratios of  $\text{Fe}^{2+}$  to  $\text{BH}_4^-$  for L-nZVI on (a) removal efficiency (b) suspended solid and (c) dissolved iron.

#### 4.1.2 pulp-modified nZVI (P-nZVI)

**Figure 4.3** illustrates effect of P-nZVI on removal efficiency. Total and residual COD removal of pulp wastewater was not effectively removal by reductive precipitation. Because real pulp wastewater may be highly pollutant such as heavy metal and ionic strength. Moreover, lignin removal from pulp and paper wastewater was low because pulp wastewater has a lot of polymers including carbohydrates, tannin, organic acids, terpenes, and resin. This is the reason why nZVI was quite not effectively removal. However, the decolorization was 85.43% that successfully removal by reductive precipitation. Chong et al.2016 demonstrated that  $Fe^0$  can completely enhance decolorization efficiency of dyes including crystal violet, methyl orange, and methylene blue. Moreover, the various forms of iron oxide including  $Fe(OH)_3$ ,  $Fe_3O_4$ ,  $Fe_2O_3$ , and  $FeOOH$  could adsorb dye molecules and enhance the decolorization of dye wastewater by generating a bridged bidentate complex (Fan et al., 2009).

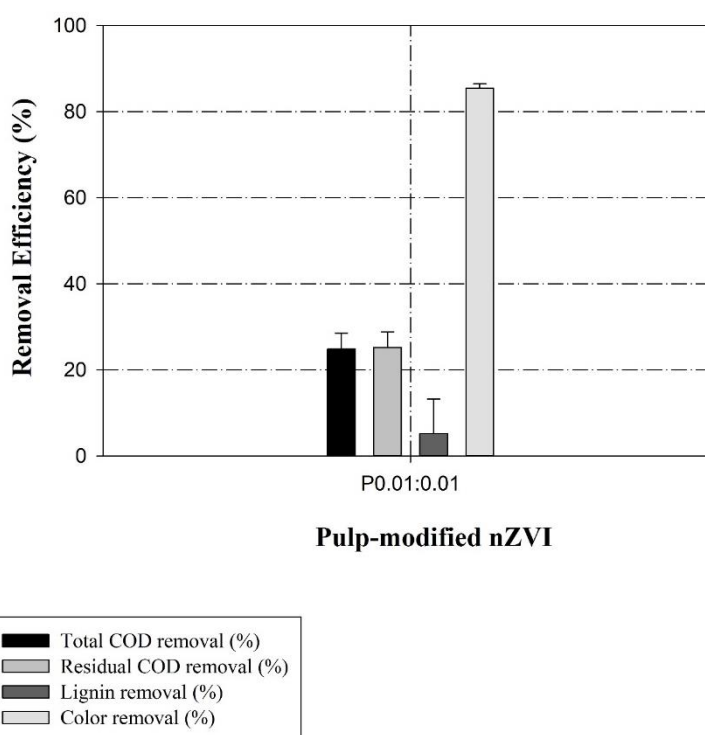


**Figure 4.3** Effect of P-nZVI on removal efficiency.

#### 4.1.3 non-modified nZVI (bare nZVI)

Bare nZVI was used the optimum mass ratio of  $\text{Fe}^{2+}$  to  $\text{BH}_4^-$  was 0.01: 0.01. The properties of bare nZVI were performed in **Table A-3**. The results were discussed in **4.1.4**.

#### 4.1.4 Comparison of various forms nZVI

Bare nZVI, L-nZVI, and P-nZVI were used at the optimum mass ratio of  $\text{Fe}^{2+}$  to  $\text{BH}_4^-$  that was 0.01: 0.01 as optimum condition.

**Table A-3** illustrates pH values of bare nZVI, L-nZVI, and P-nZVI were 6.66, 6.58, and 7.28, respectively. The pH values of bare nZVI and L-nZVI were quite similar because of similar mass of  $\text{Fe}^{2+}$  but P-nZVI was higher than them because of real wastewater. Moreover, the ORP values in nZVI solution of bare nZVI, L-nZVI, and P-nZVI were -186, -302.5, -318.5 mV, respectively. L-nZVI and P-nZVI were higher ORP values than bare nZVI because of polymer that could enhance reactivity.

**Figure 4.4 (a)** demonstrates effect of L-nZVI and P-nZVI on total and residual COD, lignin, color removal. The decolorization of L-nZVI and P-nZVI was completely removal with 92.98% and 85.43%, respectively. Therefore, this method was below the official color effluent standards. However, this method was not effective on COD removal for pulp wastewater because power of nZVI only may not be enough.

**Figure 4.4 (b)** demonstrates effect of various forms of nZVI on suspended solid. The suspended solid of L-nZVI and P-nZVI was quite similar values because these particles have polymer and higher than bare nZVI that without polymer.

**Figure 4.4 (c)** demonstrates effect of various forms of nZVI on dissolved iron. Although dissolved iron of L-nZVI was less than bare nZVI and P-nZVI, these forms of nZVI were used similar mole of  $\text{Fe}^{2+}$ . Consequently, L-nZVI may be stable than them because of pure lignin as polymer.

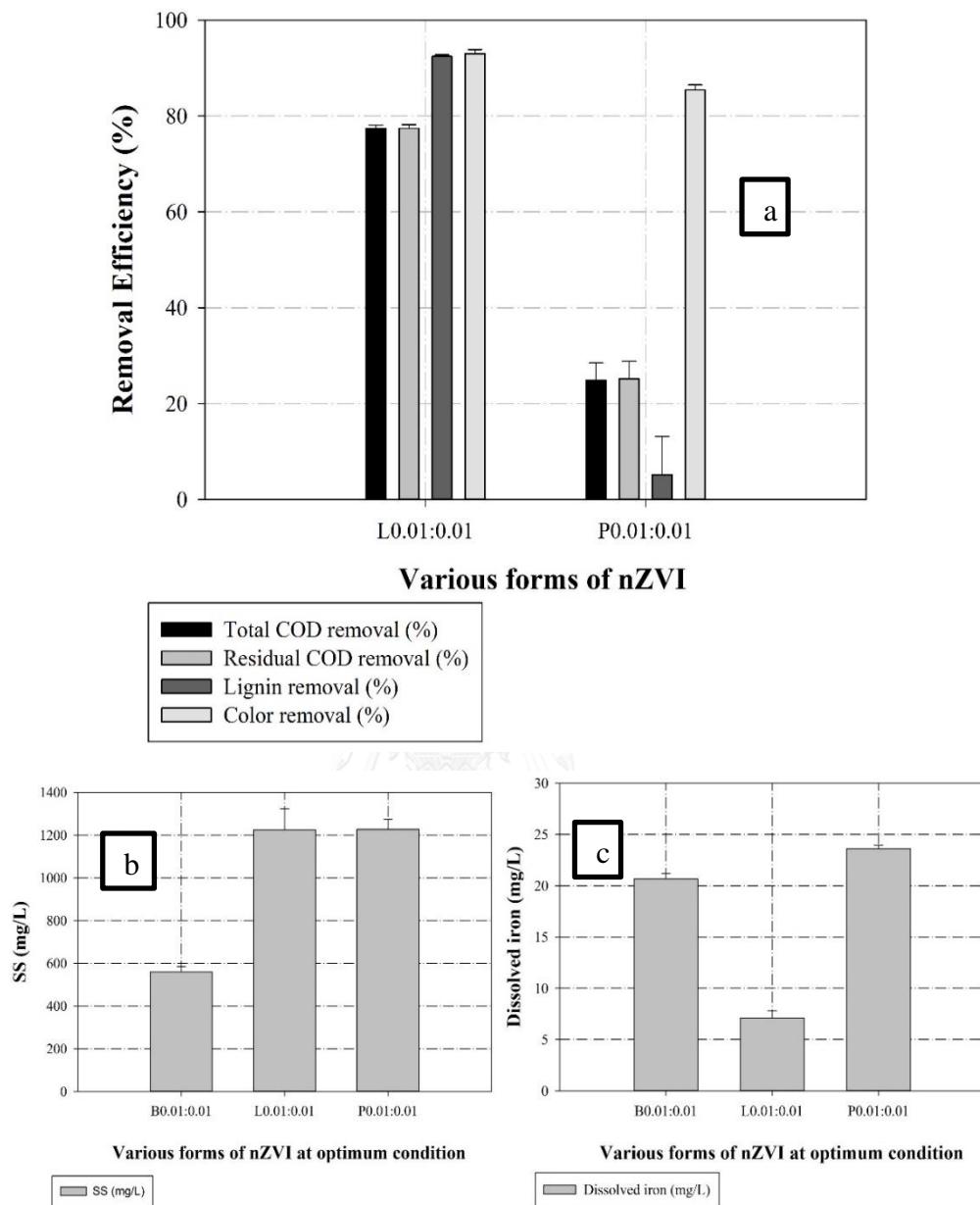


**Figure 4.4** Effect of various forms of nZVI on (a) removal efficiency, (b) suspended solid and (c) dissolved iron.

Furthermore, lignin removal was compared by using reductive precipitation and 1g/L nZVI commercial in **Figure B-1**. This result was shown that 1g/L nZVI commercial may be low sorption on lignin just 8.80 % within 5 minutes and desorption with increasing time. Because lignin removal was successfully effective by reductive precipitation and not sorption on nZVI. Therefore, post-agglomeration stabilization was lower lignin removal than pre-agglomeration stabilization as shown in **Figures 4.5 (b)** and **(d)**.

**Figure 4.5 (a)** bare nZVI or non- modified nZVI because it was used just these chemicals and the particle size of bare nZVI was quite bigger than modified-nZVI as explained in TEM results. **Figure 4.5 (c)** demonstrates a lot of polymers for pulp wastewater that coating of P-nZVI.

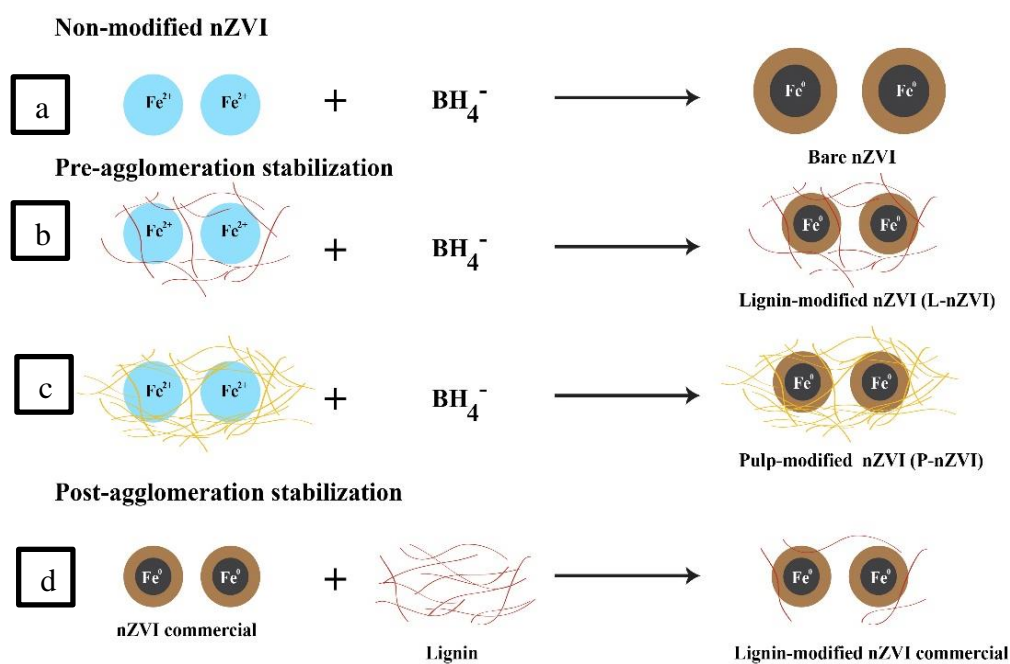


**Figure 4.5** Conceptual model for various forms of nZVI (a) bare nZVI, (b) L-nZVI, (c) P-nZVI, and (d) L-nZVI commercial.

## 4.2 Characterization of nZVI particles

### 4.2.1 Transmission electron microscopy (TEM)

**Figures 4.6 (a) to (f)** illustrates TEM images of various nZVI particles in scale 50 nm at 135 kX magnification. The average particle sizes were determined by measuring the diameter of number of particles and using IMAGEJ programs as seen **Table 4.1**.

**Table 4.1** Particle sizes of various forms of nZVI and mass ratios of  $\text{Fe}^{2+}$  to  $\text{BH}_4^-$  on lignin for L-nZVI.

Forms of nZVI	Mass ratios of $\text{Fe}^{2+}$ to $\text{BH}_4^-$	Dp (nm.)	Number of particles
B0.01:0.01	0.01:0.01	$52.72 \pm 17.58$	24
L0.01:0.01	0.01:0.01	$4.77 \pm 3.51$	140
L0.02:0.02	0.02:0.02	$2.962 \pm 2.35$	43
L0.04:0.04	0.04:0.04	$2.34 \pm 1.96$	195
L0.08:0.08	0.08:0.08	$2.14 \pm 1.56$	45
P0.01:0.01	0.01:0.01	$2.04 \pm 1.09$	40

**Figure 4.6 (a)** demonstrates that bare nZVI particles are amorphous particle with Fe core and outer shell namely iron hydroxides. These particles are spherical particles ranging diameters from 34 to 57 nm and the average of diameter is 52.72 nm. In addition, the average of diameter for bare nZVI was the biggest of diameter owing to magnetic and van der waals forces and leading to the immediately aggregation. The morphology of Bare nZVI was similar to another study (Raychoudhury et al., 2010).

The average of diameter for various L-nZVI particles were reduced particle sizes with increasing mass ratios of  $\text{Fe}^{2+}$  to  $\text{BH}_4^-$  as shown in **Table 4.1**. The average of diameter for P-nZVI was the smallest of diameter because the electrostatic and steric stabilization offered by polymer can overcome attractive van der Waals force and electric dipolar interactions between nZVI particles. Hence, the main mechanisms are polymer network and hindrance. Moreover, increasing  $\text{BH}_4^-$  concentration can create smaller size because it is reducing agent. The morphologies of L-nZVI and P-nZVI were form chain-like clusters and altered by polymer coating but different structures as can be seen in **Figures 4.6 (b) to (f)**. Furthermore, the one of the most promising methods was enhancing the performance of nZVI by polymer stabilization. Furthermore, polymer stabilization of nZVI can decrease particle agglomeration and particle size resulting in enhanced reactivity as well as mobility. Raychoudhury et al. (2010) suggested that the average particle of polyelectrolyte-stabilized nZVI is around 5 nm which is more stable and mobile than bare nZVI. The multimodal particle size distributions are induced by characteristics of polymer, including molecular weight, surface potential, and thickness of polymer layer (Ditsch et al., 2005). NZVI particle sizes depend on the synthesis method. Even though, the step in TEM sample preparation, such as drying of the NZVI suspension on the TEM grid might cause of artifacts that enhance the chance of NZVI aggregation, individual particles still occur in the images, so particle sizes can be estimated (Domingos et al., 2009). Settled out of the supernatant and bare NZVI aggregated happen rapidly because its larger size leading to higher magnetic.

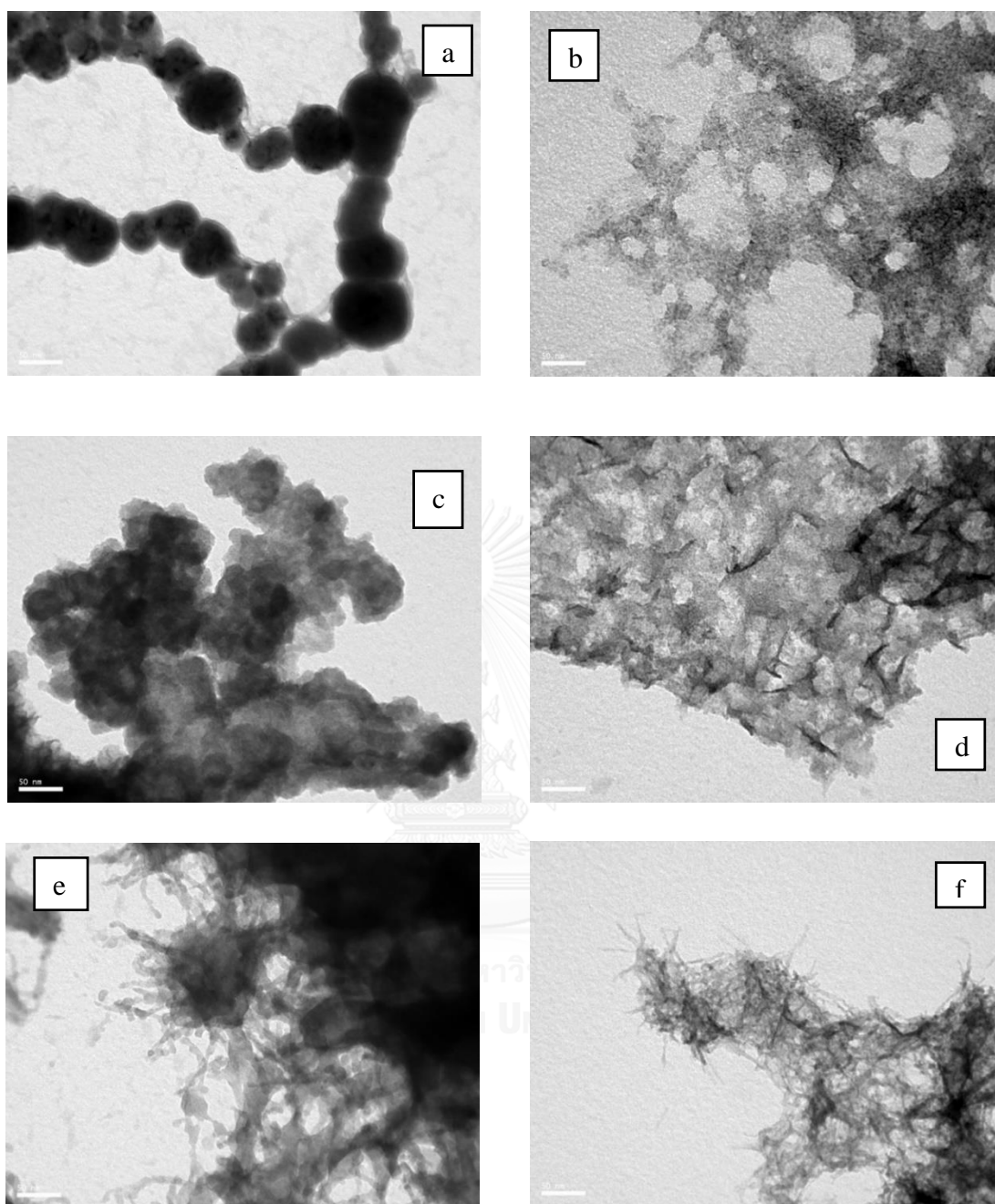


**Figure 4.6** Representative TEM images of (a) bare nZVI, (b) L0.01:0.01, (c) L0.02:0.02, (d) L0.04:0.04, (e) L0.08:0.08, and (f) P0.01:0.01 at 135 kx magnification with scale bar 50 nm.

#### 4.2.2 Scanning Electron Microscope (SEM)

Characteristic SEM images of L-nZVI and P-nZVI at similar magnification within 1000X. **Figure 4.7** illustrates SEM images of L-nZVI and P-nZVI. Some of the various mass ratios of  $\text{Fe}^{2+}$  to  $\text{BH}_4^-$  on the surface of L-nZVI or P-nZVI was so rough in **Figures 4.7 (a) to (c)**, whereas that of **Figure 4.7 (d)** L-nZVI was quite neat. Now that, various mass ratios of  $\text{Fe}^{2+}$  to  $\text{BH}_4^-$  were affected on different morphologies.

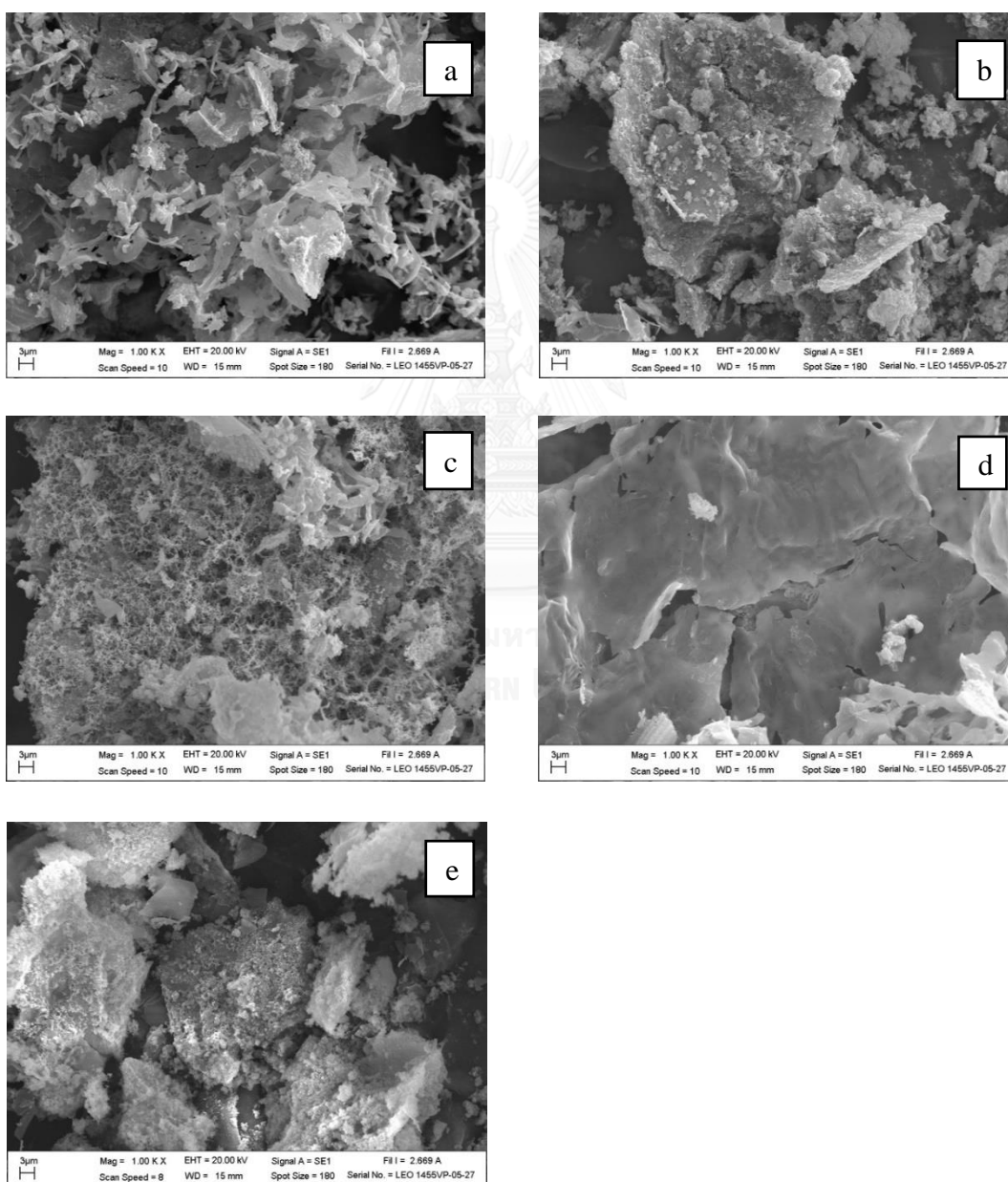


**Figure 4.7** SEM images of (a) L0.01:0.01, (b) L0.02:0.02, (c) L0.04:0.04, (d) L0.08:0.08, and (e) P0.01:0.01 at 1000X magnification.

#### 4.2.3 Energy Dispersive X-ray spectroscopy (EDX)

EDX analyses were conducted to determine the elemental components. Energy Dispersive X-ray analysis revealed peaks of Fe, O, Na, S, C, Si, and Cl in **Figure 4.8**. The elemental components between L-nZVI and P-nZVI on atomic weight percent were quite similar, whereas P-nZVI showed other components including Si and Cl. These components may be from bleaching of pulp wastewater such as  $\text{Na}_2\text{SiO}_3$ .

The ratios of components were investigated by EDX and composed of  $\frac{\text{Fe}}{\text{C}}$ ,  $\frac{\text{Fe}}{\text{O}}$ , and  $\frac{\text{Fe}}{\text{S}}$  shown in **Table 4.2** and **Figures 4.8 (a) to (e)**. The ratios of Fe to C and O for L0.01: 0.01, L0.02: 0.02, and L0.04: 0.04 were quite similar. Moreover, the ratios of Fe to C and O for L0.08: 0.08 and P0.01: 0.01 have the same tend because of their morphology in TEM result. The results demonstrated that organic compounds are the source of carbon and oxygen originates from lignin and pulp wastewater. However, sulphur from ferrous sulfate is lower than other compounds except L0.08:0.08. **Figure 4.8 (d)** that has the highest of sulphide owing to the highest amount of ferrous sulfate. Obviously, the proportion of these chemical is almost similar to iron particles.

**Table 4.2** Effect of L-nZVI and P-nZVI on Atomic weight percent by EDX.

Forms of nZVI	Atomic weight percent (%)									
	Fe	O	Na	S	C	Si	Cl	Fe/O	Fe/C	Fe/S
L0.01:0.01	21.34	27.56	5.94	8.92	36.24	-	-	0.774	0.589	2.392
L0.02:0.02	17.5	24.76	3.01	2.68	52.05	-	-	0.707	0.336	6.530
L0.04:0.04	15.56	22.05	2.48	2.03	57.87	-	-	0.706	0.269	7.665
L0.08:0.08	8.57	47.96	10.23	10.77	22.48	-	-	0.179	0.381	0.796
P0.01:0.01	10.15	34.90	2.61	1.90	48.64	0.69	1.10	0.291	0.209	5.342

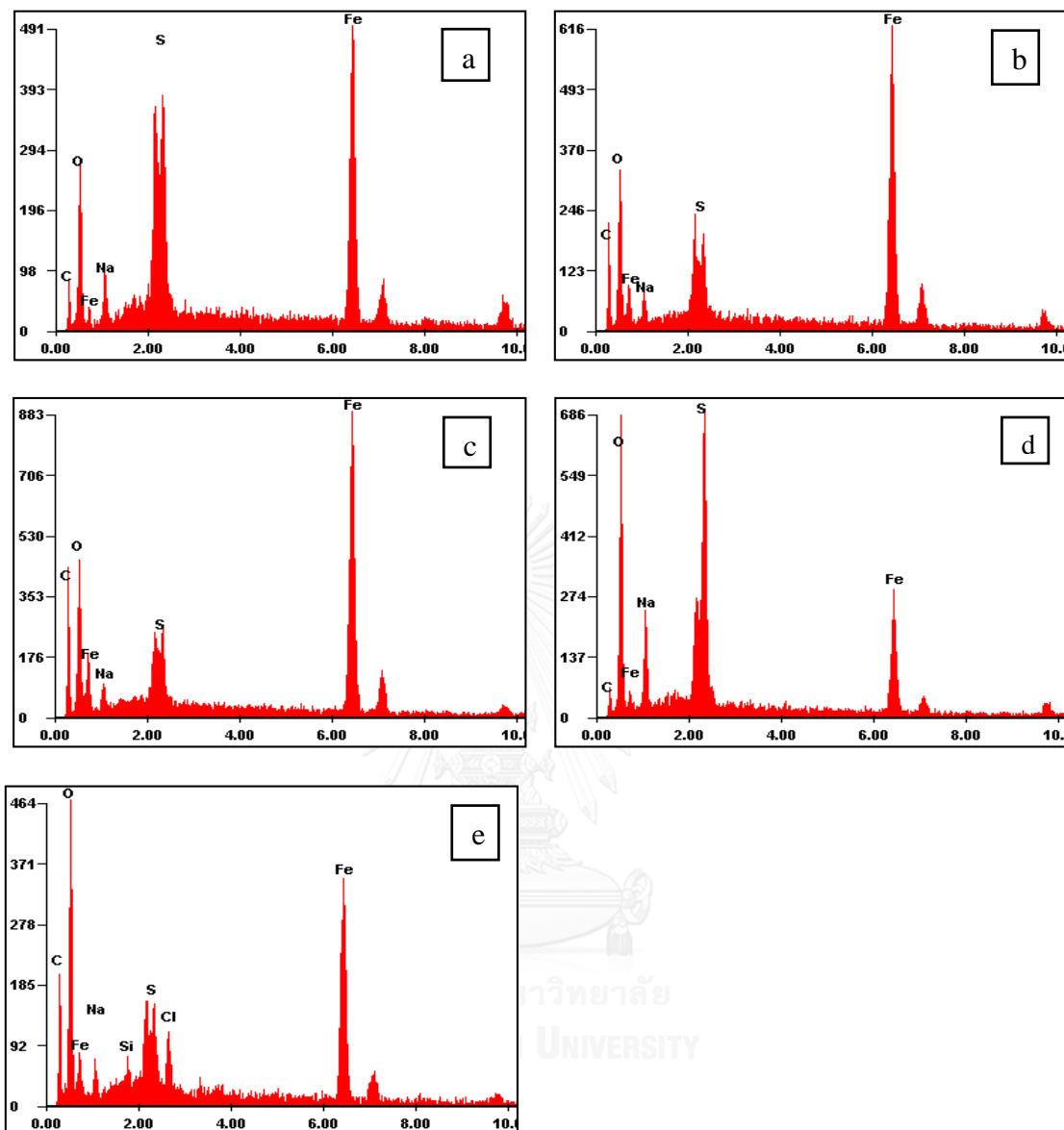


**Figure 4.8** EDX analyses of (a) L0.01:0.01, (b) L0.02:0.02, (c) L0.04:0.04, (d) L0.08:0.08, and (e) P0.01:0.01.

#### 4.2.4 X-ray powder diffraction (XRD)

Various precipitated forms, composed of  $\text{Fe}(\text{OH})_3$ ,  $\text{Fe}(\text{OH})_2$ ,  $\text{Fe}_3\text{O}_4$ ,  $\text{Fe}_2\text{O}_3$ ,  $\text{FeOOH}$ , and green rusts, could be mixture of amorphous either iron oxyhydroxide, ferrous, or ferric oxide by during corrosion reactions. These forms are depending on the pH and redox conditions of the system and been as sorbents only according to the following **Equation 2-4** to **2-10** and related the resulting of XRD as **Figures 4.9 (a)** to **(d)** illustrate not only various mass ratios of  $\text{Fe}^{2+}$  to  $\text{BH}_4^-$  of L-nZVI but also P-nZVI contained significant amorphous of iron oxide. The various iron forms were zero valent state(Fe), lepidocrocite ( $\gamma\text{-FeOOH}$ ), goethite( $\alpha\text{-FeOOH}$ ), maghemite ( $\gamma\text{-Fe}_2\text{O}_3$ ), and magnetite( $\text{Fe}_3\text{O}_4$ ) with the peaks at 2theta were  $45.26^\circ$ ,  $31.80^\circ$ ,  $34.72^\circ$ , and  $75.03^\circ$ , respectively. Williams and Scherer (2001) suggested that the maghemite and magnetite peaks are quite similar due to their lattice parameters are so similar. All peaks were quite alike many researchers (Garcia et al., 2016; Liang et al., 2014; Mosafer et al., 2014; Sun et al., 2006, and Kanel et al., 2005). In apart from, some peaks were different and similar of 2theta owing to various mass ratios of  $\text{Fe}^{2+}$  to  $\text{BH}_4^-$  and wastewater. Li et al. (2007) suggested that the oxygen species were detected at the surface of iron oxides (i.e., goethite and hematite) in water. Previous study suggests that the composition of the oxide shell depends on the synthesis processes and environmental conditions. Nanoparticles derived from the metallic vapour nucleation consist of  $\gamma\text{-Fe}_2\text{O}_3$  or  $\text{Fe}_3\text{O}_4$ , with higher  $\gamma\text{-Fe}_2\text{O}_3$  for small particles due to faster oxidation reactions. Whereas, nanoparticles from goethite and hematite reaction, hydrogen gas on particle contain a  $\text{Fe}_3\text{O}_4$  shell. The occurrence of wustite (FeO) has also been recommended. Iron nanoparticles generated from sodium borohydride reduction of iron salts, only a few research about the surface characterization has been investigated. Based on our previous work, the oxide shell could be described as FeOOH.

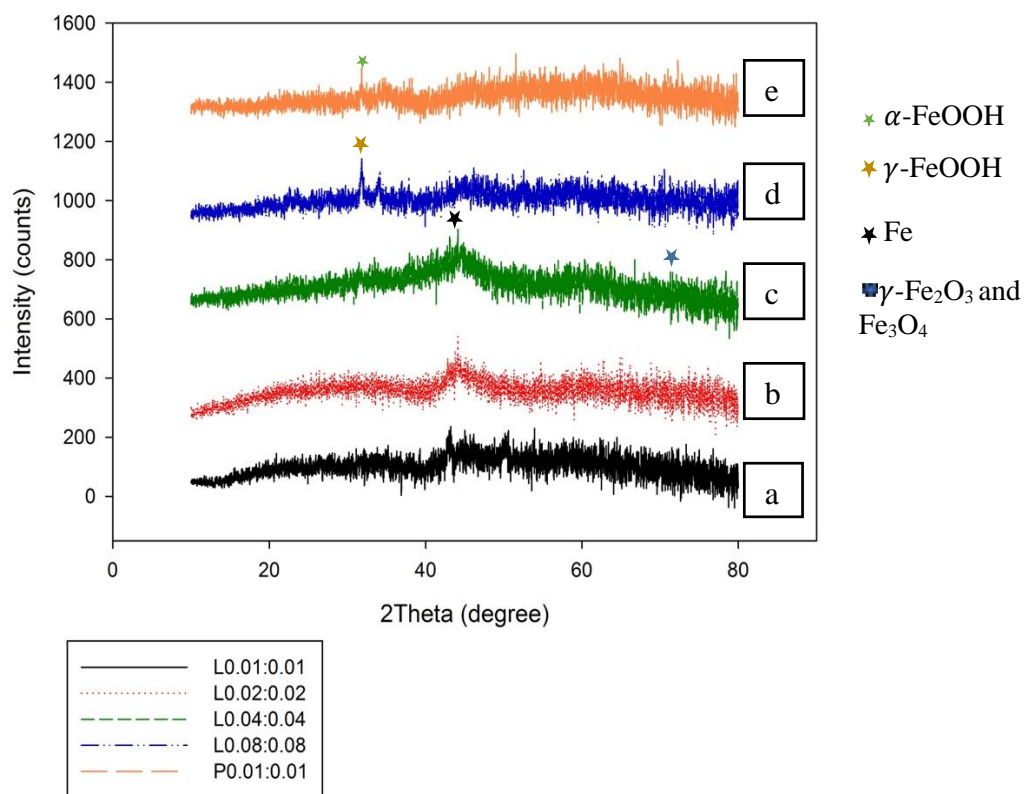


**Figure 4.9** XRD patterns of (a) L0.01:0.01, (b) L0.02:0.02, (c) L0.04:0.04, (d) L0.08:0.08, and (e) P0.01:0.01.

#### 4.2.5 Brunauer-Emmett-Teller (BET)

The specific surface areas of nZVI were determined by using BET method. **Figure 4.10** demonstrates the specific surface area of P-nZVI quantified by BET was  $49.36 \text{ m}^2/\text{g}$ , which is greater than all L-nZVI particles that were 7.61, 11.37, 12.58, and  $13.32 \text{ m}^2/\text{g}$  with increasing mass ratios of  $\text{Fe}^{2+}$  to  $\text{BH}_4^-$ . Therefore, the increased surface area to the different morphologies of L-nZVI and P-nZVI. Although, P-nZVI was synthesized by optimum condition, pulp wastewater has a lot of polymers including lignin and starch, while alkali lignin consists of lignin only. Moreover, suspended solids of pulp wastewater and pure alkali lignin were  $111 \text{ mg/L}$ , and  $0 \text{ mg/L}$ , respectively. These are the reason why P-nZVI was higher the specific surface area than L-nZVI at optimum condition. Furthermore, the specific surface area of bare nZVI was quite lower than L-nZVI and P-nZVI at similar the ratio and depended on diameter size as mention before. Therefore, this study was successfully enhanced the specific surface area by lignin and pulp wastewater modified nZVI. Furthermore, the sorption of hetero-macromolecules could lead to the greater specific surface area of P-nZVI in comparison to L-nZVI.

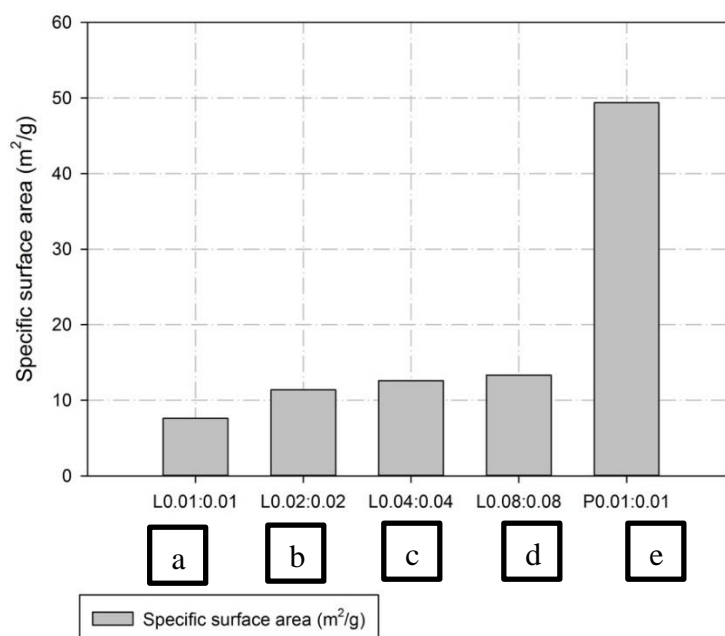


**Figure 4.10** BET surface area of (a) L0.01:0.01, (b) L0.02:0.02, (c) L0.04:0.04, (d) L0.08:0.08, (e) P0.01:0.01.

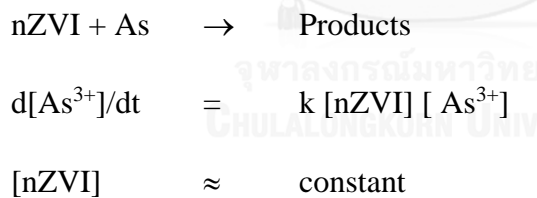
### 4.3 Arsenic removal by nZVI

In this part, L-nZVI (4 mass ratios), bare nZVI (optimum condition), and P-nZVI (optimum condition) were used to remove arsenic (III) from the synthetic wastewater.

#### 4.3.1 Lignin-modified nZVI

##### 4.3.1.1 Open system

**Figures 4.11 (a), (b), and (c)** illustrate the effect of L0.01:0.01, L0.02:0.02, L0.04:0.04, and L0.08:0.08 on total arsenic removal, pH, and ORP of the sample having initial arsenic concentration of 1 mg/L, and pH of  $7 \pm 0.06$ . Kinetics of arsenic removal was determined using first- and second-order rate laws and found that the observed data could be fitted better by first-order kinetics. This is understandable since the nZVI dosage used in this experimental part was much higher than the concentration of arsenic in the synthetic wastewater (1 g/L vs 1 mg/L). Hence, the amount of nZVI present in the solution was in excess and was considerably constant when compared with the concentration of arsenic. Therefore, the rate law could be simply described by the pseudo-first order reaction with respect to arsenic as proposed in the following equations.



$$\therefore \frac{d[\text{As}^{3+}]}{dt} = k_{\text{obs}} [\text{As}^{3+}]$$

$$\text{As}_t = \text{As}_0 e^{-k_{\text{obs}} t}$$

Which can be expressed as

$$\ln\left(\frac{\text{As}_t}{\text{As}_0}\right) = -k_{\text{obs}} t$$

$$\text{Half-life} = \frac{\ln 2}{k}$$

where,  $As_t$  = The residual total arsenic concentration at time  $t$ ,  
 $As_0$  = The initial total arsenic concentration at time 0,  
 $k_{obs}$  = the pseudo-first kinetic rate constant ( $\text{min}^{-1}$ )

The kinetic rate constants of various forms of L-nZVI were enhanced by increasing mass ratios of  $\text{Fe}^{2+}$  to  $\text{BH}_4^-$  as showed in **Table 4.3**

**Table 4.3** The pseudo first-order rate constant of total arsenic removal and half-life in various forms of nZVI.

Forms of nZVI	$k_{obs}$ ( $\text{min}^{-1}$ )	Half-life (min)	$R^2$
B0.01:0.01	0.50	1.4	0.8207
L0.01:0.01	0.39	1.8	0.9190
L0.02:0.02	0.70	1.0	0.9990
L0.04:0.04	0.78	0.9	0.7935
L0.08:0.08	1.26	0.5	0.7982
P0.01:0.01	0.51	1.4	0.9532

As can be seen in **Figure 4.11 (a)**, total arsenic removal efficiency by L0.01:0.01, L0.02:0.02, L0.04:0.04, and L0.08:0.08 were 88.66%, 96.98%, 96.49%, and 99.57%, respectively within 5 minutes. Interestingly, when time increased to 60 minutes, the arsenic removal efficiency decreased to 1.15%, 10.59%, 89.13%, and 83.30% for L0.01:0.01, L0.02:0.02, L0.04:0.04, and L0.08:0.08, respectively. Because all samples have changed arsenic form to be non-dissolved arsenic.

**Figures 4.11 (b) and (c)** reveal the decrease of pH and the increase of ORP respectively, for all nZVI evaluated in this study. This trend agrees with the slow depletion of the nZVI similar to results reported previously (Waclawek et al., 2015). As can be seen in **Equation. 2-11**, ferric oxide reacts with arsenite species that generated proton, decreasing the pH of the system. In almost all of L0.01:0.01,

L0.02:0.02, L0.04:0.04, and L0.08:0.08 the pH values decreased essentially from 7 to 4.82, 4.70, 4.50, and 4.36, respectively. However, with increasing time, ORP values of L0.01:0.01, L0.02:0.02, L0.04:0.04, and L0.08:0.08 were escalated similarly and approximately from 144 to 213, 211.5, 217, and 208, respectively. These results can confirm various arsenic forms with changing ORP and pH.

According to the pH and ORP, the predominant arsenic (III) species in all nZVI reactors should be  $\text{H}_3\text{AsO}_3$  as illustrated in **Figure 4.12**. Thus, arsenic removal mechanism is the inner-sphere and outer -sphere complexation between ferric hydroxide surface and arsenite species as suggested by (Phenrat et al., 2007), and also shows in **Equations (2-11) to (2-16)**, respectively.



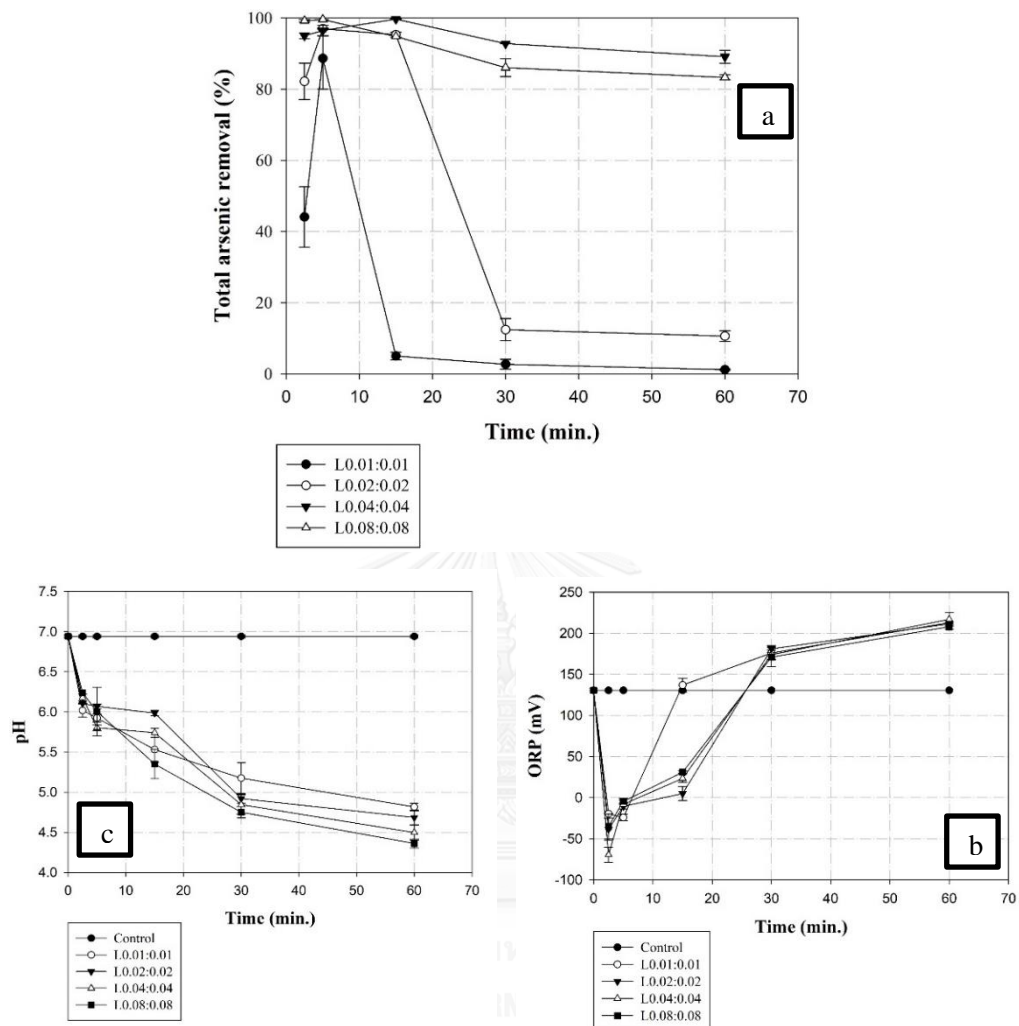


**Figure 4.11** Effect of the various mass ratios of  $\text{Fe}^{2+}$  to  $\text{BH}_4^-$  for L-nZVI on (a) total arsenic removal, (b) pH, and (c) ORP within 2.5, 5, 15, 30, and 60 minutes.

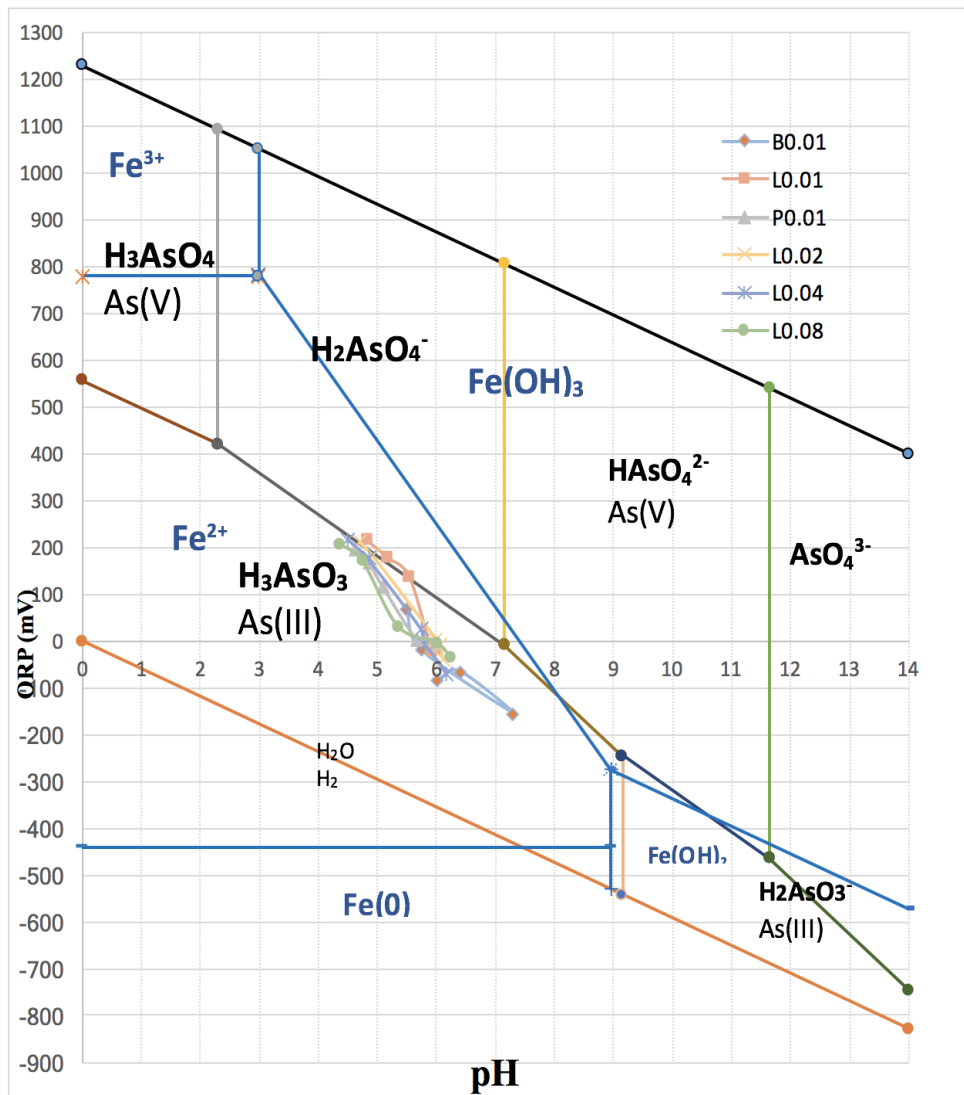


**Figure 4.12** ORP-pH diagram for the As-Fe-H<sub>2</sub>O in various forms of nZVI within 2.5, 5, 15, 30, 60 minutes at 25°C, 1 bar total pressure.

#### 4.3.1.2 Closed system

In this study was taken the sample just one time only at 60 minutes. It can be explained limited oxygen or close system.

As can be seen in **Figure 4.13 (a)**, total arsenic removal efficiency by L0.01:0.01, L0.02:0.02, L0.04:0.04, and L0.08:0.08 were 46.32%, 82.35%, 90.24%, and 92.62%, respectively at 60 minutes. Moreover, dissolved arsenic removal efficiency by L0.01:0.01, L0.02:0.02, L0.04:0.04, and L0.08:0.08 were 96.93%, 98.36%, 98.59%, and 95.010%, respectively at 60 minutes.

As a result, in **Figure 4.13 (b)** could confirm the further reduction of As(III) species to non-dissolved arsenic as shown in **Equations 2-20 to 2-22**. The non-dissolved arsenic of L0.01:0.01, L0.02:0.02, L0.04:0.04, and L0.08:0.08 were 0.232, 0.073, 0.038, 0.011 mg/L. The decreased non-dissolved arsenic at 1 g/L L-nZVI was caused by various particle structures as shown in characterization of TEM, SEM, EDX, and XRD. **Figure 4.13 (c) and (d)** reveal the decrease of pH and the increase of ORP respectively within 60 minutes, for all nZVI evaluated in this study. This trend agrees with the slow depletion of the nZVI similar to results reported previously.

**Figure 4.14** nZVI can generate hydrogen gas that might be enhanced arsenic removal because of oxidation-reduction potential as can be seen in **Equations 2-23 to 2-25**. Therefore, hydrogen can be oxidized by  $\text{H}_2\text{AsO}_3^-$ , and  $\text{HAsO}_3^{2-}$ , which are reduced. These pathways can support to arsenic removal by nZVI and hydrogen.

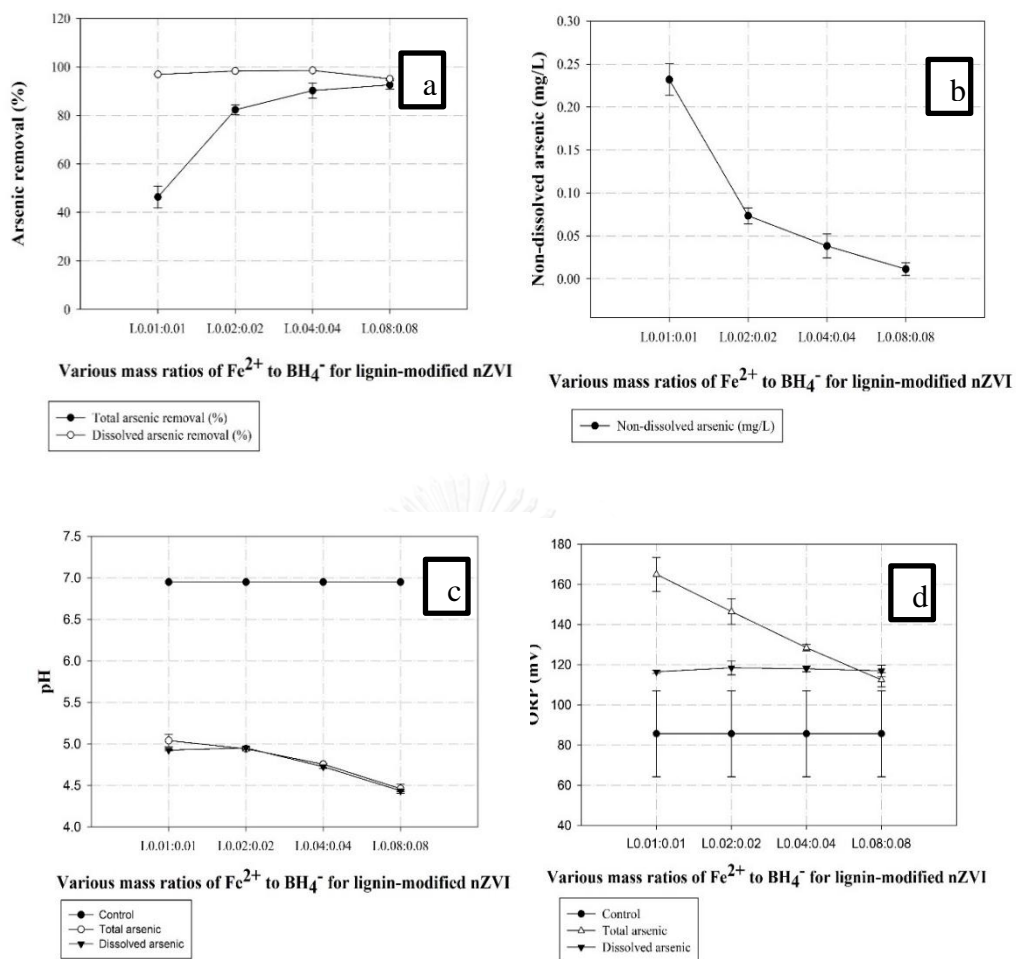


**Figure 4.13** Effect of the various mass ratios of  $\text{Fe}^{2+}$  to  $\text{BH}_4^-$  for L-nZVI on (a) total and dissolved arsenic removal, (b) non-dissolved arsenic, (c) pH, and (d) ORP at 60 minutes.

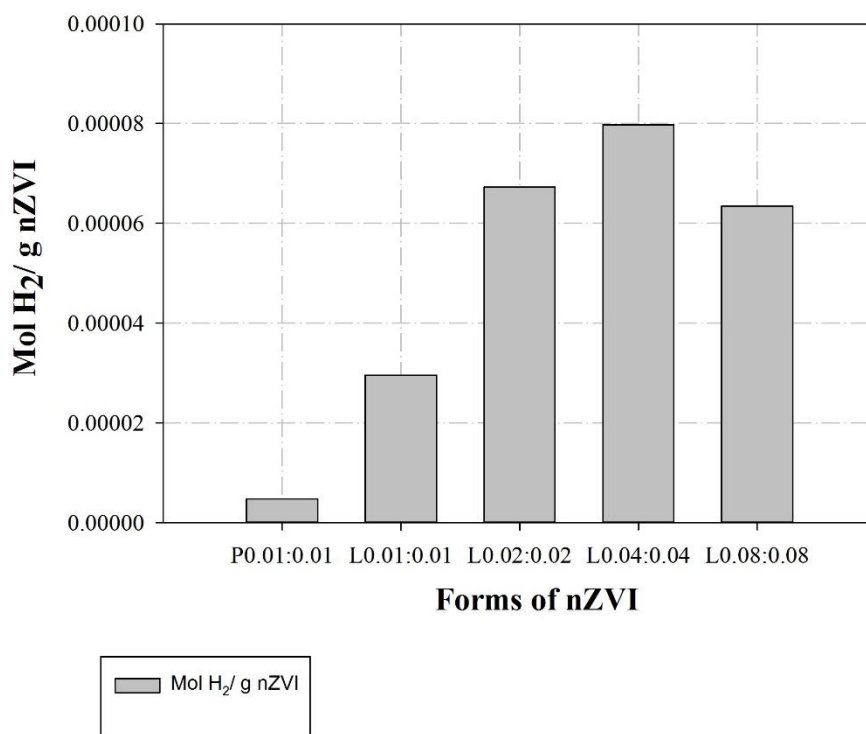


**Figure 4.14** Effect of various forms of nZVI on hydrogen production.

#### 4.3.1.3 Comparison

**Figure 4.15** demonstrates comparison between open and closed system of the various mass ratios of  $\text{Fe}^{2+}$  to  $\text{BH}_4^-$  for L-nZVI on (a) total arsenic removal, (b) pH, and (c) ORP at 60 minutes. Total arsenic removal efficiency and pH values in closed system were higher than open system as shown in **Figure 4.15 (a)** and **(b)**. However, ORP values in closed system were lower than open system as shown in **Figure 4.15 (c)**.

This finding suggests that the solution chemistry of the batch experiment might change because the experiment was opened to the atmosphere. Consequently, dissolved oxygen may increase and oxidize nZVI particle that is loss surface area of nZVI resulting in the decreased of arsenic removal efficiency using nZVI.

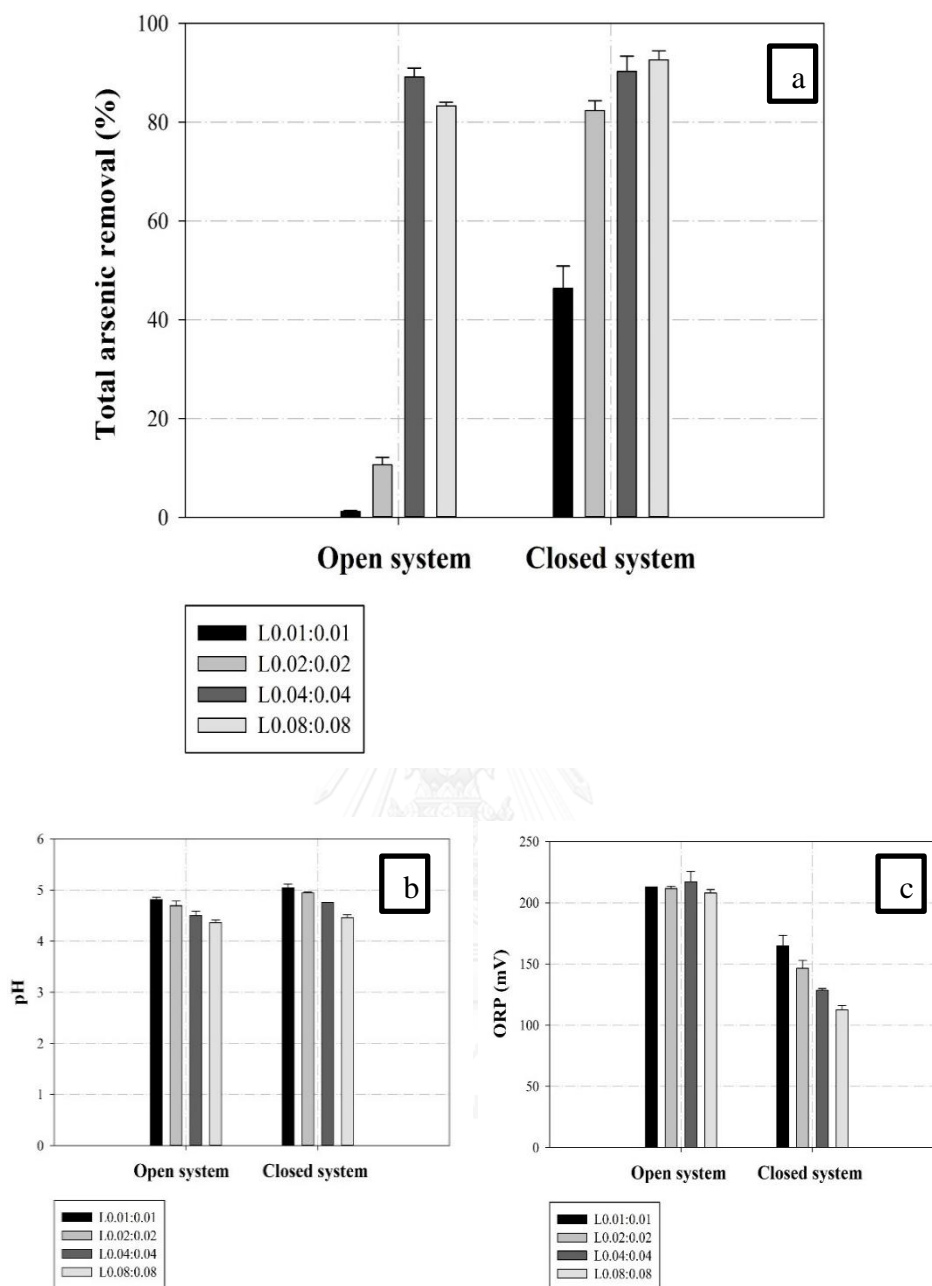


**Figure 4.15** Comparison between open and closed system of the various mass ratios of  $\text{Fe}^{2+}$  to  $\text{BH}_4^-$  for L-nZVI on (a) total arsenic removal, (b) pH, and (c) ORP at 60 minutes.

### 4.3.2 Various forms of nZVI

Bare nZVI, L-nZVI, and P-nZVI at optimum condition were used to remove arsenic (III) from the synthetic wastewater.

#### 4.3.2.1 Open system

**Figures 4.16 (a), (b), and (c)** illustrate the effect of bare nZVI, L-nZVI, and P-nZVI on total arsenic removal, pH, and ORP of the sample having initial arsenic concentration of 1 mg/L, and pH of  $7 \pm 0.06$ . The observed pseudo first-order rate constants and half-lives in of the experiments are reported in **Table 4.3**. The pseudo first-order rate constants of P-nZVI ( $k_{\text{obs}}$  of  $0.5101 \text{ min}^{-1}$ ), were higher than bare nZVI ( $k_{\text{obs}}$  of  $0.5012 \text{ min}^{-1}$ ), and L-nZVI ( $k_{\text{obs}}$  of  $0.3949 \text{ min}^{-1}$ ), respectively. The kinetic of arsenic removal by L- nZVI and P- nZVI might be significant complex because of lignin or polymer composition. Arsenic concentration varies with time, indicated arsenic desorption reaction occur at the surface. The fast adsorption rates might contribute strong adsorption performance of nZVI deposite on the nZVI surface. Hence, lignin molecules and arsenic could be adsorbed on its particle.

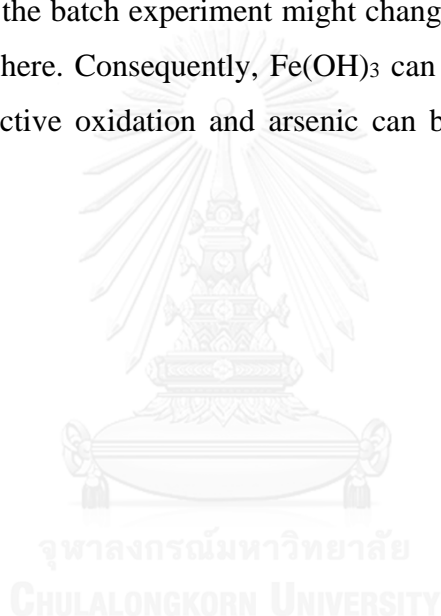
As can be seen in **Figure 4.16 (a)**, total arsenic removal efficiency by bare nZVI, L-nZVI, and P-nZVI were 88.79%, 88.66%, and 90.79%, respectively within 5 minutes. Furthermore, the sorption of hetero-macromolecules could lead to the greater specific surface area of P-nZVI in comparison to L-nZVI. Consequently, P-nZVI can enhance arsenic removal more than that of L-nZVI at optimum condition. Interestingly, when time increased to 60 min, the arsenic removal efficiency decreased to 82.07%, 1.15%, and 65.87% for bare nZVI, L-nZVI, and P-nZVI, respectively.

**Figure 4.16 (b)** and **(c)** reveal the decrease of pH and the increase of ORP respectively, for all nZVI evaluated in this study. This trend agrees with the slow depletion of the nZVI similar to results reported previously. As can be seen in **Equation. 2-11**, ferric oxide reacts with arsenite species that generated proton, decreasing the pH of the system.

In almost all of bare nZVI, L-nZVI, and P-nZVI the pH values decreased essentially from 7 to 5.49, 4.82, and 4.62, respectively. However, with increasing time, ORP values

of bare nZVI, L-nZVI, and P-nZVI were escalated similarly and approximately from 144 to 69, 213, and 192.5, respectively.

**Figures 4.17** demonstrate conceptual model for arsenic removal by various forms of nZVI **(a)** L-nZVI, **(b)** P-nZVI, and **(c)** bare nZVI. All results of arsenic for various forms were confirmed that when increased time, arsenic solution could be non-dissolved arsenic. Therefore, this research was separated dissolved and non-dissolved arsenic by filter. Moreover, nZVI may be created thin iron oxide layer including magnetite and maghemite by increasing time. In addition, this finding suggests that the solution chemistry of the batch experiment might change because the experiment was opened to the atmosphere. Consequently,  $\text{Fe}(\text{OH})_3$  can be suspended particles in the system as further reactive oxidation and arsenic can be absorbed on  $\text{Fe}(\text{OH})_3$  with increasing time also.



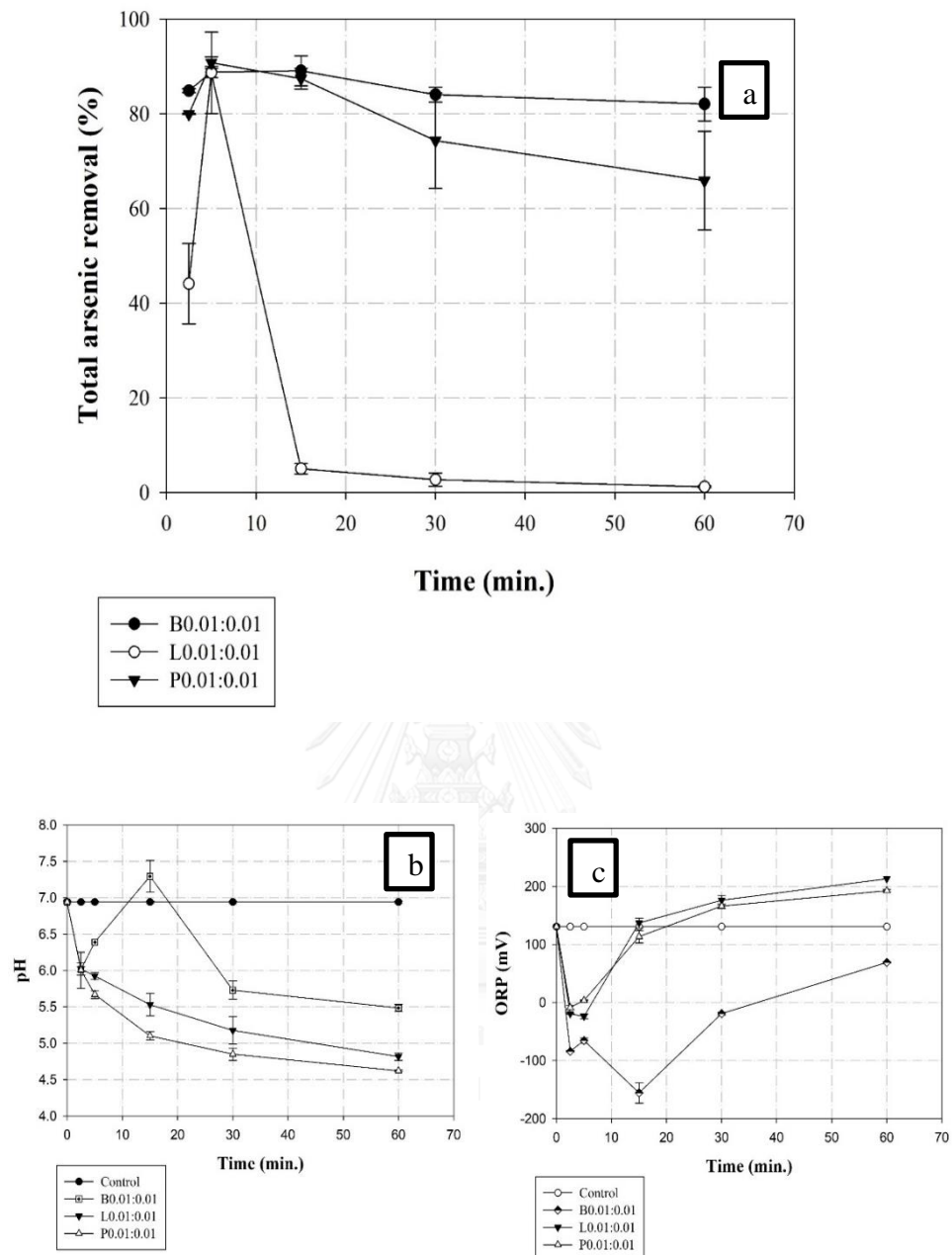


**Figure 4.16** Effect of the various forms of nZVI on (a) total arsenic removal, (b) pH, and (c) ORP within 2.5, 5, 15, 30, and 60 minutes.

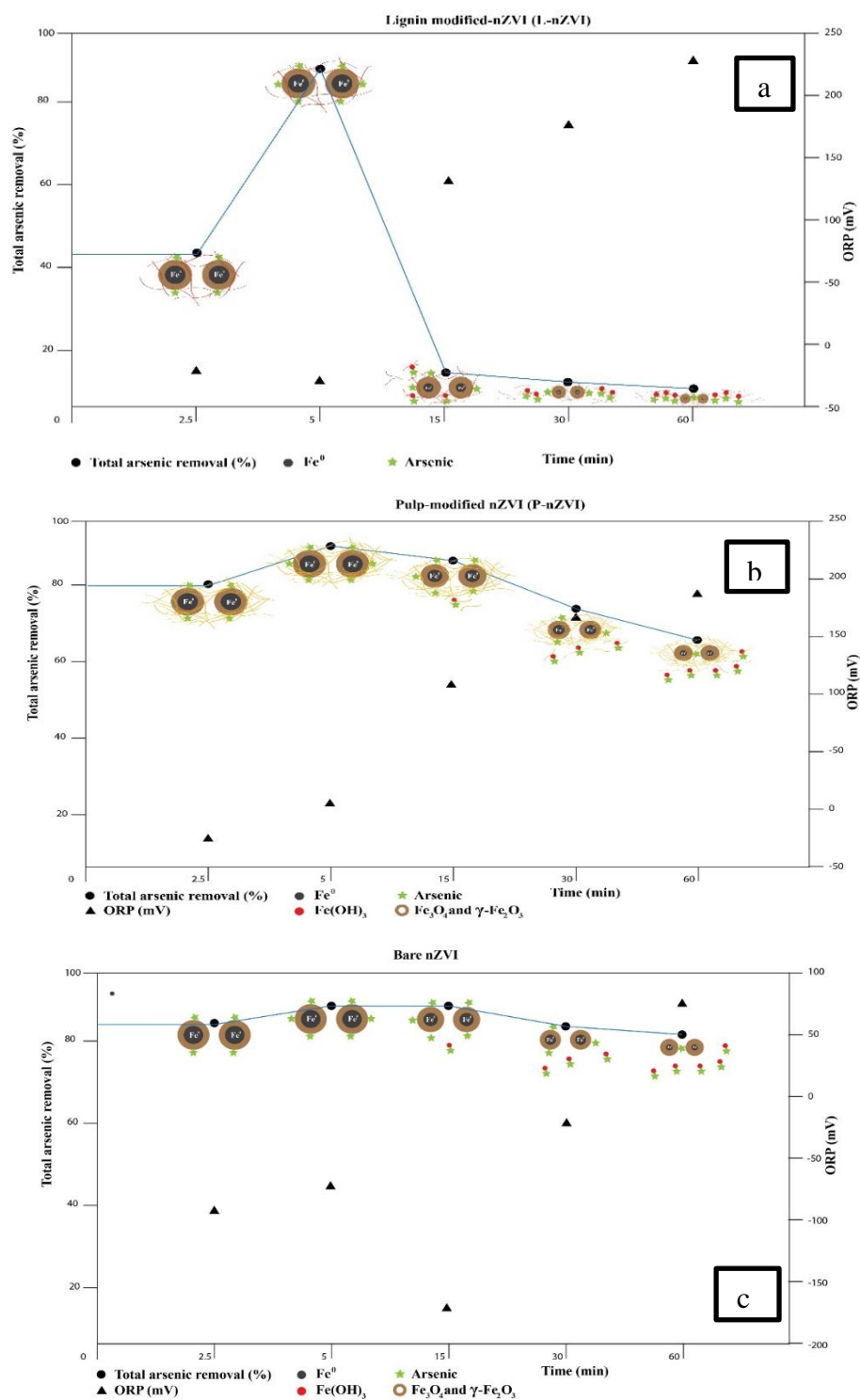


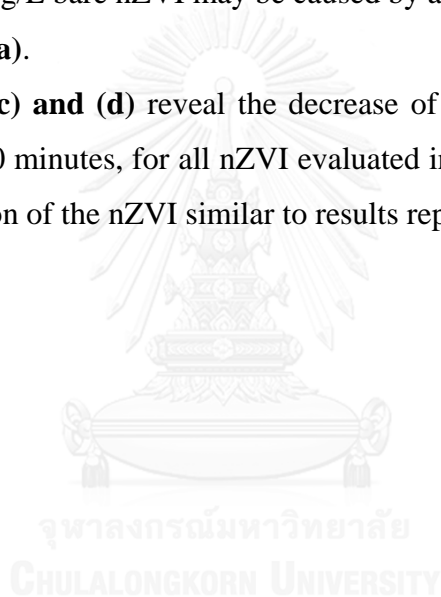
**Figure 4.17** Conceptual model for total arsenic removal by various forms of nZVI (a) L-nZVI, (b) P-nZVI, and (c) bare nZVI.

#### 4.3.2.2 Closed system

As can be seen in **Figure 4.18 (a)**, total arsenic removal efficiency by bare nZVI, L-nZVI, and P-nZVI were 85.15%, 46.32%, and 47.06%, respectively within 60 minutes. Moreover, dissolved arsenic removal efficiency by bare nZVI, L-nZVI, and P-nZVI were 85.43%, 96.93%, and 81.51%, respectively within 60 minutes.

**Figure 4.18 (b)** could confirm the further reduction of As(III) species to non-dissolved arsenic as shown in **Equation 2-20** to **2-22**. The non-dissolved arsenic of bare nZVI, L-nZVI, and P-nZVI were 0.0001, 0.232, and 0.0140 mg/L. The decreased non-dissolved arsenic at 1 g/L bare nZVI may be caused by aggregation of particle as TEM image in **Figure 4.6 (a)**.

**Figure 4.18 (c) and (d)** reveal the decrease of pH and the increase of ORP respectively within 60 minutes, for all nZVI evaluated in this study. This trend agrees with the slow depletion of the nZVI similar to results reported previously.



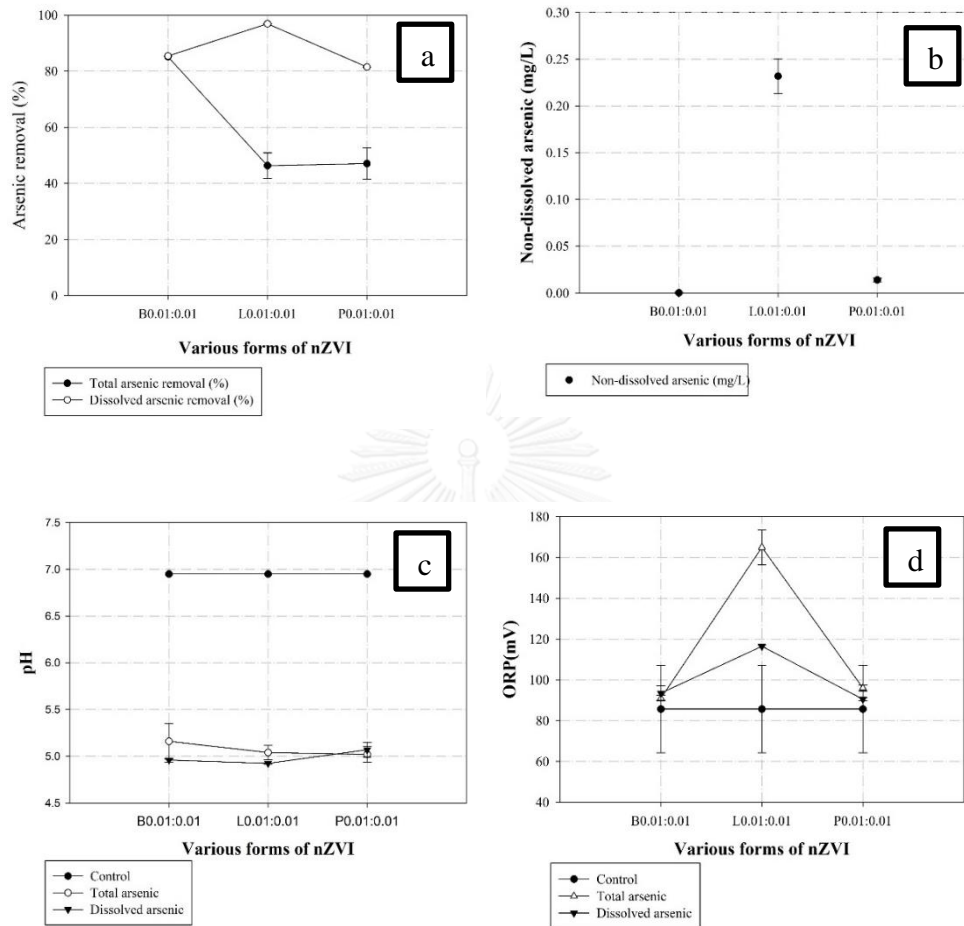


**Figure 4.18** Effect of the various forms of nZVI on (a) total and dissolved arsenic removal, (b) non-dissolved arsenic, (c) pH, and (d) ORP at 60 minutes.

#### 4.3.2.3 Comparison

**Figure 4.19** demonstrates comparison between open and closed system of the various forms of nZVI on (a) total arsenic removal, (b) pH, and (c) ORP at 60 minutes. The arsenic removal efficiency of closed system for bare nZVI and L-nZVI were higher than open system except P-nZVI as shown in **Figure 4.19 (a)**. However, pH values of closed system for L-nZVI and P-nZVI were quite higher than open system except bare nZVI as shown in **Figure 4.19 (b)**. Moreover, ORP values of open system for L-nZVI and P-nZVI were higher than closed system except bare nZVI. This finding was mentioned before.



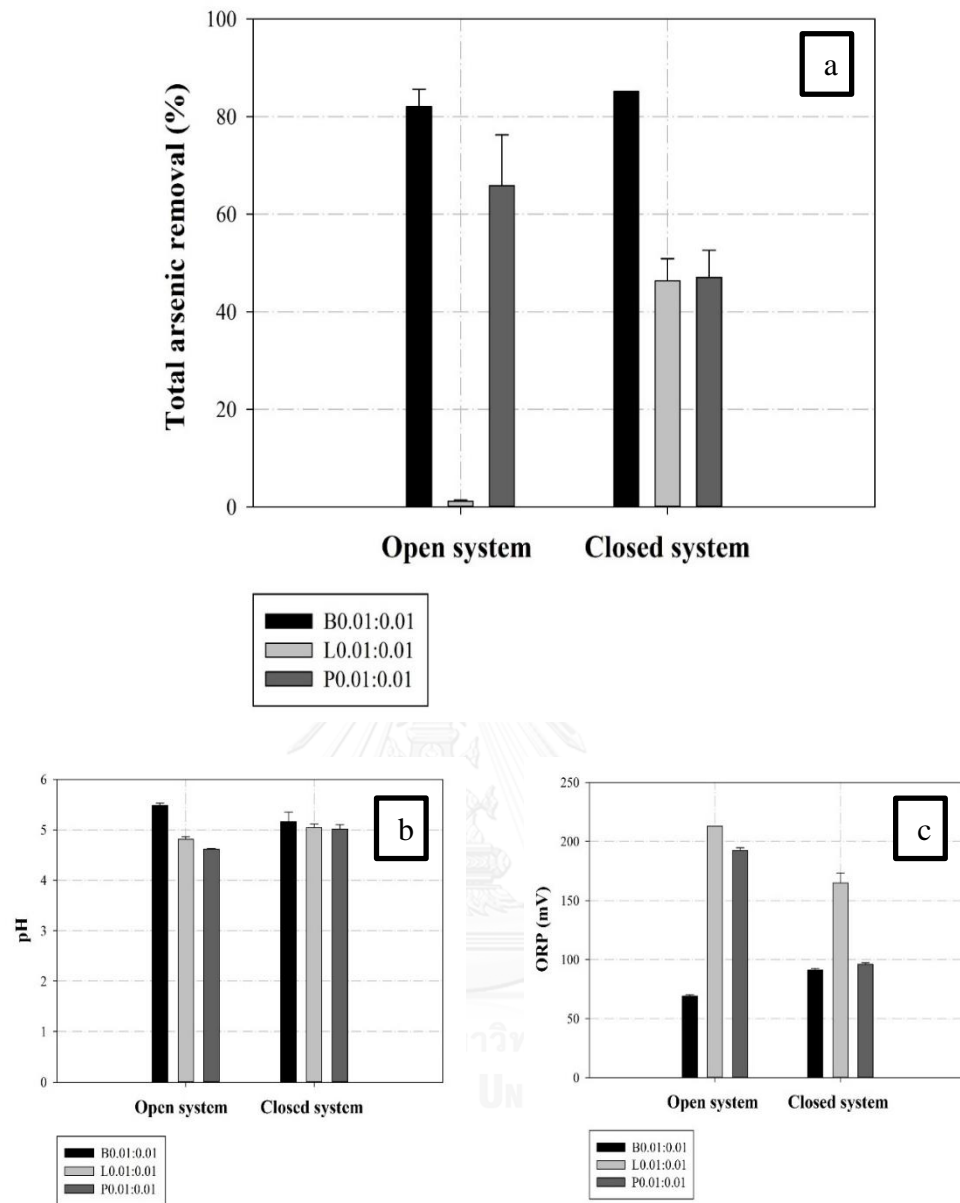


**Figure 4.19** Comparison between open and closed system of the various forms of nZVI on (a) total arsenic removal, (b) pH, and (c) ORP at 60 minutes.

## CHAPTER V

### CONCLUSION AND RECOMMENDATIONS

#### 5.1 Conclusion

This research was able to remove lignin and color using reductive precipitation and able to produce lignin-modified nZVI (L-nZVI) and pulp-modified nZVI (P-nZVI) as by-products. The optimum molar ratio of  $\text{Fe}^{2+}$  to  $\text{BH}_4^-$ , 0.01:0.01, led to the highest lignin, color, and COD removal percentages of 92.40%, 92.98%, and 77.44%, respectively. Moreover, P-nZVI could reduce the color of the pulp wastewater from 2,130 to 96 ADMI, which is in compliance with the proposed new effluent standard of 300 ADMI. Moreover, lignin coating both in L-nZVI and P-nZVI can enhance nZVI properties, leading to smaller diameter particle, higher specific surface area, and better total arsenic removal. Regarding on arsenic removal, the B-nZVI, L-nZVI, and P-nZVI at 1 g/L could remove 88.79%, 88.66%, and 90.79%, respectively, of 1 mg/L total arsenic in 5 minutes.

#### 5.2 Recommendations

1. The oxidation states and speciation of arsenic removed by the synthesized nZVI should be further investigated to better understand the removal mechanism of arsenic in the presence of nZVI.
2. Behavior of nZVI in arsenic removal under anaerobic and flow conditions similar to those occurs in groundwater should be investigated.

## REFERENCES

- Aghdam, M. A., Kariminia, H. R., & Safari, S. (2016). Removal of lignin, COD, and color from pulp and paper wastewater using electrocoagulation *Desalination and Water Treatment*, 57, 9698-9704.
- Allabaksh, M. B., Mandal, B. K., Kesarla, M. K., Kumar, K. S., & Pamanji, S. R. (2010). Preparation of stable zerovalent iron nanoparticles using different chelating agents. *J. Chem. Pharm. Res*, 2, 67-74.
- Anawar, H. M., Akai, J., Mostofa, K. M. G., Safiullah, S., & Tareq, S. M. (2002). Arsenic poisoning in groundwater: Health risk and geochemical sources in Bangladesh *Environ. Int.*, 277, 597-604.
- Bang, S., MD., J., Korfiatis, G. P., & Meng, X. (2005). Chemical reactions between arsenic and zero-valent iron in water *water research*, 39, 763-770.
- Basavegowda, N., & Lee, Y. R. (2013). Synthesis of silver nanoparticles using Satsuma mandarin (Citrus unshiu) peel extract: A novel approach towards waste utilization. *Materials Letters*, 109, 31-33.
- Bezbaruah, A. N., Krajangpan, S., Chisholm, B. J., Khan, E., & Bermudez, J. J. (2009). Entrapment of iron nanoparticles in calcium alginate beads for groundwater remediation applications. *J. Hazard. Mater*, 166, 1339-1343.
- Bouajila, J., Dole, P., Joly, C., & Limare, A. (2006). Some laws of a lignin plasticization *J. Appl. Polym. Sci*, 102, 1445-1451.
- Chiu, V. Q., & Hering, J. G. (2000). Arsenic adsorption and oxidation at manganite surfaces. 1. Method for simultaneous determination of adsorbed and dissolved arsenic species *Environ. Sci. Technol*, 34, 2029-2034.
- Choi, H. C., Giasuddin, A. M., & Kanel, S. R. (2008). Method of synthesizing air-stable zerovalent iron nanoparticles at room temperature and applications. *US Patent*, 11, 889-896.
- Crane, R. A., & Scott, T. B. (2012). Nanoscale Zero-Valent Iron: Future Prospects for an Emerging Water Treatment Technology *J. Hazard. Mater*, 211-212, 112-125.
- Farrell, J., Wang, J., O'Day, P., & Coklin, M. (2001). Electrochemical and spectroscopic study of arsenate removal from water using zerovalent iron media. *Environ. Sci. Technol*, 35, 2026-2032.
- Ferguson, J. F., & Garvis, J. (1972). Review of the arsenic cycle in natural waters. *water research*, 6, 1259-1274.
- Garcia, A., Toledano, A., Andres, M. A., & Labidi, J. (2010). Study of the antioxidant capacity of Miscanthus sinensis lignins. *Process Biochemistry*, 45, 935-940.
- Geng, B., Jin, Z., Li, T., & Qi, X. (2009). Kinetics of hexavalent chromium removal from water by chitosan-Fe<sub>0</sub> nanoparticles. *Chemosphere*, 75, 825-830.
- Grieger, K. D., Fjordbøge, A., Hartmann, N. B., Eriksson, E., Bjerg, P. L., & Baun, A. (2010). Environmental benefits and risks of zerovalent iron nanoparticles (nZVI) for in situ remediation: risk mitigation or trade-off. *J. Contam. Hydrol*, 118, 165-183.
- Gurses, A., Karaca, S., Dogar, C., Bayrak, R., Acikyildiz, M., & Yalcin, M. (2004). Determination of adsorptive properties of clay/water system: methylene blue sorption. *J. Colloid Interface Sci*, 269, 310-314.

- Hambardzumyana, A., Foulon, L., Bercu, N. B., Pernes, M., Maigret, J. E., Molinari, M., . . . Beghin, V. A. (2015). Organosolv lignin as natural grafting additive to improve the water resistance of films using cellulose nanocrystals. *Chemical Engineering Journal*, 264, 780-788.
- He, F., & Zhao, D. (2005). Preparation and characterization of a new class of starch-stabilized bimetallic nanoparticles for degradation of chlorinated hydrocarbons in water. *Environ. Sci. Technol*, 39, 3314–3320.
- Joo, S. H., Feitz, A. J., & Waite, T. D. (2004). Oxidative degradation of the carbothioate herbicide, molinate, using nanoscale zero-valent iron. *Environ. Sci. Technol*, 38, 2242-2247.
- Kalyani, K. S. P., Balasubramanian, P., & Srinivasakannan, C. (2009). Decolorization and COD reduction of paper industrial effluent using electro-coagulation. *Chem. Eng. J*, 151, 97-104.
- Kanel, S. R., Nepal, D., Manning, B., & Choi, H. (2007). Transport of surface-modified iron nanoparticle in porous media and application to arsenic (III) remediation *J. Nanopart. Res*, 9, 725-735.
- Kanel., Manning, B., Charlet, L., & Choi, H. (2005). Removal of Arsenic(III) from Groundwater by Nanoscale Zerovalent Iron. *Environ. Sci. Technol*, 39, 1291-1298.
- Katsoyiannis, I. A., Ruettimann, T., & Hug, S. J. (2008). pH dependence of Fenton reagent generation and As(III) oxidation and removal by corrosion of zero valent iron in aerated water. *Environmental Science and Technology*, 42 7424-7430.
- Kindsigo, M., & Kallas, J. (2006). Degradation of lignins by wet oxidation: model water solutions. *Proc. Estonian Acad. Sci. Chem*, 55(3), 132-144.
- Kumar, P., Tow, T. T., Chand, S., & Wasewar, K. L. (2011). Treatment of Paper and Pulp Mill Effluent by Coagulation. *International Journal of Chemical, Molecular, Nuclear, Materials and Metallurgical Engineering*, 5, 715-720.
- Lackovic, J. A., Nikolaidis, N. P., & Dobbs, G. M. (2000). Inorganic arsenic removal by zerovalent iron. *Environ. Eng. Sci*, 17, 29-39.
- Laumann, S., Micic, V., & Hofmann., T. (2014). Mobility enhancement of nanoscale zerovalent iron in carbonate porous media through co- injection of polyelectrolytes. *water research*, 50, 70-79.
- Li, J., Zhao, X., Shi, Y., Cai, Y., Mou, S., & Jiang, G. (2008). Mixed hemimicelles solid-phase extraction based on cetyltrimethylammonium bromide-coated nano-magnets Fe<sub>3</sub>O<sub>4</sub> for the determination of chlorophenols in environmental water samples coupled with liquid chromatography/spectrophotometry detection. *Journal of Chromatography A*, 1180(1-2), 24–31.
- Liang, W., Dai, C., Zhou, X., & Zhang, Y. (2014). Application of Zero-Valent Iron Nanoparticles for the Removal of Aqueous Zinc Ions under Various Experimental Conditions. *Plos one*, 9.
- Lien, H. L., & Zhang, W. (1999). Transformation of chlorinated methanes by nanoscale iron particles. *J. Environ. Eng*, 125, 1042-1047.
- Liu, Y. Q., & Lowry, G. V. (2006). Effect of particle age (Fe-o content) and solution pH on NZVI reactivity: H-2 evolution and TCE dechlorination. *Environ. Sci. Technol.*, 40 6085–6090.

- Manning, B. A., Hunt, M., Amrhein, C., & Yarmoff, J. A. (2002). Arsenic(III) and arsenic(V) reactions with zerovalent iron corrosion products. *Environ. Sci. Technol*, 36, 5455-5461.
- Milczarek, G., Rebis, T., & Fabianska, J. (2013). One-step synthesis of lignosulfonate-stabilized silver nanoparticles *Coll. Surf. Biointerf*, 105, 335-341.
- Mosaferi, M., Nemati, S., Khataee, A., Nasser, S., & Hashemi, A. A. (2014). Removal of Arsenic (III, V) from aqueous solution by nanoscale zerovalent iron stabilized with starch and carboxymethyl cellulose *Journal of Environmental Health Science & Engineering*.
- Mostashari, S. M., Shariati, S., & Manoochehri, M. (2013). Lignin removal from aqueous solutions using Fe<sub>3</sub>O<sub>4</sub> magnetic nanoparticles as recoverable adsorbent *Cellulose Chemistry and Technology*, 47, 727-734.
- Mulder, W. J., Gosselink, R. J. A., Vingerhoeds, M. H., Harmsen, P. F. H., & Eastham, D. (2011). Lignin based controlled release coatings. *Industrial Crops and Products*, 34, 915-920.
- NevarezL, A. M., Casarrubias, L. B., Celzard, A., Fierro, V., Munoz, V. T., Davila, A. C., . . . Sanchez, G. G. (2011). Biopolymer-based nanocomposites: effect of lignin acetylation in cellulose triacetate films *Sci. Technol. Adv. Mater*, 12, 1-16.
- Ng, J. C., Wang, J., & Shraim, A. (2003). A global health problem caused by arsenic from natural sources *Chemosphere*, 529, 1353-1359.
- Nyman, V., Rose, G., & Ralston, J. (1986). The colloidal behaviour of kraft lignin and lignosulfonates. *Coll. Surf*, 21, 125-147.
- O'Carroll, D., Sleep, B., Krol, M., Boparai, H., & Kocur, C. (2013). Nanoscale zerovalent iron and bimetallic particles for contaminated site remediation. *Advances in Water Resources*, 51, 104-122.
- Pang, Y. X., Qiu, X. Q., Yang, D. J., & Lou, H. M. (2008). Influence of oxidation, hydroxymethylation and sulfomethylation on the physicochemical properties of calcium lignosulfonate. *Coll. Surf. A: Physicochem Eng. Asp*, 312(2-3), 154-159.
- Phenrat, T., Saleh, N., Sirk, K., Tilton, R. D., & Lowry, G. V. (2007). Aggregation and sedimentation of aqueous nanoscale zerovalent iron dispersions. *Environ. Sci. Technol*, 41, 284-290.
- Ponder, S. M., Darab, J. C., & Mallouk, T. E. (2000). Remediation of Cr(VI) and Pb(II) aqueous solutions using supported, nanoscale zerovalent iron. *Environ. Sci. Technol*, 34, 2564-2569.
- Ramos, M. A. V., Yan, W., Li, X. Q., Koel, B. E., & Zhang, W. X. (2009). Simultaneous oxidation and reduction of arsenic by zerovalent iron nanoparticles: understanding the significance of the core-shell structure. *J Phys Chem C*, 113, 14591-14594.
- Ravenscroft, P., Brammer, H., & Richards, K. (2009). *Arsenic Pollution: A Global Synthesis*.
- Saleh, N., Kim, H. J., Phenrat, T., Matyjaszewski, K., Tilton, R. D., & Lowry, G. V. (2008). Ionic strength and composition affect the mobility of surface-modified Fe<sub>0</sub> nanoparticles in water saturated sand columns *Environ. Sci. Technol*, 42, 3349-3355.

- Sirk, K. M., Saleh, N. B., Phenrat, T., Kim, H. J., Dufour, B., Ok, J., . . . Tilton, R. D. (2009). Effect of adsorbed polyelectrolytes on nanoscale zerovalent iron particle attachment to soil surface models. *Environ. Sci. Technol*, *43*, 3803-3808.
- Smedley, P. L., & Kinniburgh, D. G. (2002). A review of the source, behaviour and distribution of arsenic in natural waters. *Appl. Geochem*, *17*, 517-568.
- Stefaniuk, M., Oleszczuk, P., & Ok, S. Y. (2016). Review on nano zerovalent iron (nZVI): From synthesis to environmental applications *Chemical Engineering Journal*, *287*, 618-632.
- Su, C., & Puls, R. W. (2001). Arsenate and arsenite removal by zerovalent iron: effects of phosphate, silicate, carbonate, borate, sulfate, chromate, molybdate, and nitrate, relative to chloride. *Environ. Sci. Technol*, *35*, 4562-4568.
- Tiraferri, A., & Sethi, R. (2009). Enhanced transport of zerovalent iron nanoparticles in saturated porous media by guar gum *J. Nanopart. Res*, *11*, 635-645.
- Tucek, J., Pucek, R., Kolarik, J., Zoppellaro, G., Petr, M., Filip, J., . . . R., Z. (2017). Zero-Valent Iron Nanoparticles Reduce Arsenites and Arsenates to As(0) Firmly Embedded in Core-Shell Superstructure: Challenging Strategy of Arsenic Treatment under Anoxic Conditions. *ACS Sustainable Chem*, *5*, 3027-3038.
- Tyrovola, K., Peroulaki, E., & Nikolaidis, N. P. (2007). Modeling of arsenic immobilization by zero valent iron. *European Journal of Soil Biology*, *43*, 356-367.
- Voegelin, A., & Hug, S. J. (2003). Catalyzed oxidation of arsenic(III) by hydrogen peroxide on the surface of ferrihydrite: an in situ ATR-FTIR study. *Environ. Sci. Technol*, *37*, 972-978.
- Wang, X., Chen, C., Liu, H., & Ma, J. (2008). Preparation and characterization of PAA/ PVDF membrane-immobilized Pd/Fe nanoparticles for dechlorination of trichloroacetic acid *water research*, *42*, 4656-4664.
- Wu, L., & Ritchie, S. M. C. (2006). Removal of trichloroethylene from water by cellulose acetate supported bimetallic Ni/Fe nanoparticles *Chemosphere*, *63*, 285-292.
- Xie, L., & Shang, C. (2005). Role of humic acid and quinine model compounds in bromated reduction by zerovalent iron *Environ. Sci. Technol*, *39*, 1092-1100.
- Yaich, L. A., Edlund, U., & Albertsson, A. C. (2012). Wood hydrolysate barriers: performance controlled via selective recovery. *Biomacromolecules*, *13*, 466-473.
- Yan, W. L., Ramos, M. A. V., Koel, B. E., & Zhang, W. X. (2010). Multi-tiered distributions of arsenic in iron nanoparticles: Observation of dual redox functionality enabled by a core-shell structure *Chem Commun*, *46*, 6995-6997.
- Zhang, W. (2003). Nanoscale iron particles for environmental remediation: An overview *J. Nanopart. Res*, *5*, 323-332.
- Zhu, B. W., Lim, T. T., & Feng, J. (2008). Influences of amphiphiles on dechlorination of a trichlorobenzene by nanoscale Pd/Fe: adsorption, reaction kinetics, and interfacial interactions *Environ. Sci. Technol*, *42*, 4513-4519.

## APPENDIX



จุฬาลงกรณ์มหาวิทยาลัย  
CHULALONGKORN UNIVERSITY

## Appendix A: Properties of nZVI

**Table A-1** Lignin-modified nZVI (L-nZVI)

Sample	Before removing nZVI					
	Ratio of Fe <sup>2+</sup> to BH <sub>4</sub> <sup>-</sup>	pH	ORP (mV)	DO (mg/L)	Temperature (°C)	Conductivity (ms/cm)
1 g/L lignin	-	8.43±0.085	59±3.606	7.53 ±0.202	25.6 ±1.082	0.255 ±0.003
L0.01:0.005	0.01:0.005	6.87±0.014	-172.5 ±4.950	0.345 ±0.021	24.75 ±0.071	2.27 ±0.028
L0.01:0.01	0.01:0.01	6.58±0.099	-302.5 ±3.536	0.217 ±0.090	26.1 ±0.265	2.51 ±0.042
L0.01:0.02	0.01:0.02	7.22±0.482	-292 ±2.828	0.223 ±0.061	25.3 ±0.173	3.06 ±0.04
L0.01:0.04	0.01:0.04	9.11±0.127	-388.5 ±3.536	0.253 ±0.029	26.33 ±0.723	4.69 ±0.044
L0.01:0.08	0.01:0.08	9.65±0.042	-458.67 ±25.007	0.34 ±0.014	34.1 ±0.141	8.26 ±0.106
L0.02:0.02	0.02:0.02	6.39±0.227	-321 ±12.728	0.217 ±0.067	26.4 ±0.400	4.413 ±0.076
L0.04:0.04	0.04:0.04	6.09±0.055	-336 ±22.627	0.207 ±0.032	26.8 ±0.557	7.753 ±0.097
L0.08:0.08	0.08:0.08	6.00±0.061	-373 ±33.941	0.23 ±0.053	27	13.49 ±0.118

Sample	After removing nZVI					
	Ratio of Fe <sup>2+</sup> to BH <sub>4</sub> <sup>-</sup>	pH	ORP (mV)	DO (mg/L)	Temperature (°C)	Conductivity (ms/cm)
L0.01:0.005	0.01:0.005	5.62±0.106	-48 ±9.899	1.33 ±0.198	23.15 ±0.212	2.29 ±0.0141
L0.01:0.01	0.01:0.01	4.87±0.106	-4.5 ±2.121	1.51 ±0.266	24.8 ±0.436	2.477 ±0.038
L0.01:0.02	0.01:0.02	7.17±0.125	-189.3 ±8.386	0.21 ±0.090	24 ±0.608	3.017 ±0.042
L0.01:0.04	0.01:0.04	9.19±0.053	-155 ±14.142	1.18 ±0.440	24.37 ±0.666	4.623 ±0.012
L0.01:0.08	0.01:0.08	9.72±0.021	-378.5 ±13.435	0.56 ±0.077	31.4 ±0.283	8.17 ±0.198
L0.02:0.02	0.02:0.02	4.95±0.099	-25.5 ±12.021	0.76 ±0.191	24.63 ±0.306	4.367 ±0.085
L0.04:0.04	0.04:0.04	5.04±0.119	-61 ±35.355	1.74 ±0.275	24.63 ±0.231	7.663 ±0.099
L0.08:0.08	0.08:0.08	5.40±0.283	-40.5 ±4.950	0.447 ±0.247	25.17 ± 0.153	13.187 ±0.357

**Table A-2** Pulp-modified nZVI (P-nZVI)

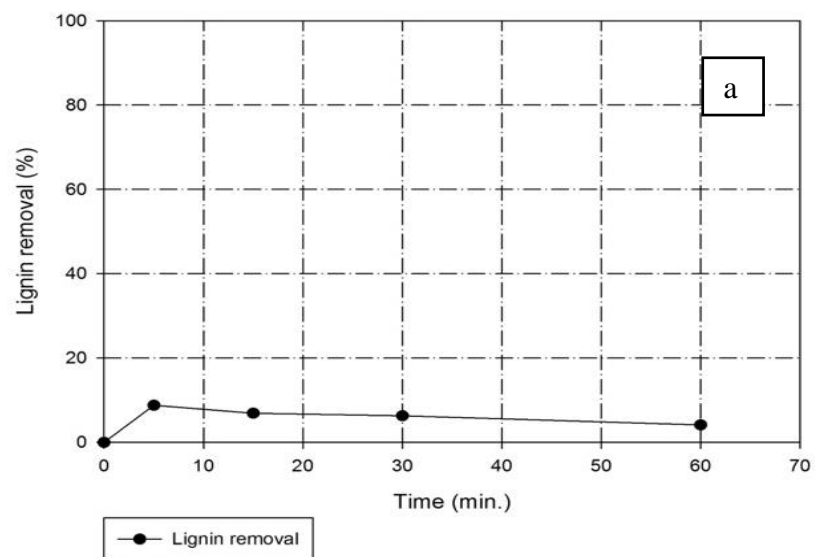
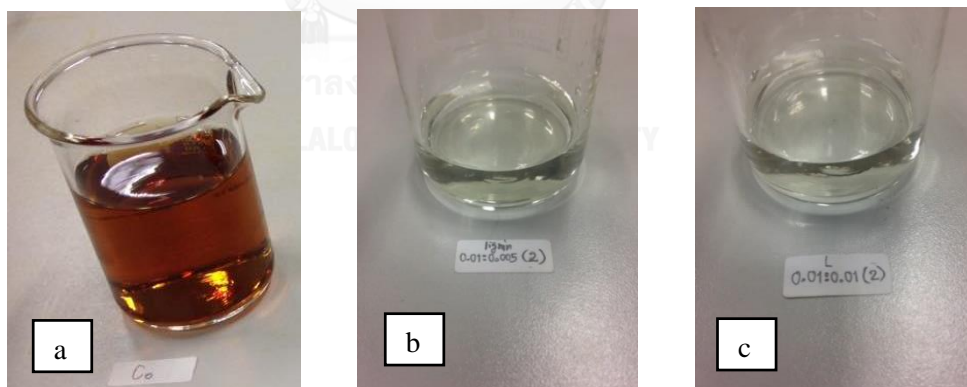
Sample	Before removing nZVI					
	Ratio of Fe <sup>2+</sup> to BH <sub>4</sub> <sup>-</sup>	pH	ORP (mV)	DO (mg/L)	Temperature (°C)	Conductivity (ms/cm)
Pulp wastewater	-	6.09	141	2.87	26.4	2.55
P0.01:0.01	0.01:0.01	7.28±0.198	-318.5 ±13.435	0.33 ±0.007	28.4 ±0.141	4.05

Sample	After removing nZVI					
	Ratio of Fe <sup>2+</sup> to BH <sub>4</sub> <sup>-</sup>	pH	ORP (mV)	DO (mg/L)	Temperature (°C)	Conductivity (ms/cm)
P0.01:0.01	0.01:0.01	6.25±0.042	-104 ±2.828	0.3	24.15 ±0.212	3.975 ±0.021

**Table A-3** Bare nZVI (B-nZVI)

Sample	Before removing nZVI					
	Ratio of Fe <sup>2+</sup> to BH <sub>4</sub> <sup>-</sup>	pH	ORP (mV)	DO (mg/L)	Temperature (°C)	Conductivity (ms/cm)
DI water	-	7.02±0.137	217.2 ±1.980	7.02 ±0.137	25.3	0.002
B0.01:0.01	0.01:0.01	6.66±0.049	-186 ±2.828	0.17 ±0.014	27.7 ±0.141	2.43

Sample	After removing nZVI					
	Ratio of Fe <sup>2+</sup> to BH <sub>4</sub> <sup>-</sup>	pH	ORP (mV)	DO (mg/L)	Temperature (°C)	Conductivity (ms/cm)
B0.01:0.01	0.01:0.01	5.78±0.106	-138.5 ±6.364	0.6	25.5	2.46 ±0.028

**Appendix B:** lignin removal by nZVI commercial and color removal.**Figure B-1 (a)** 1 g/L Lignin removal by 1g/L nZVI commercial.

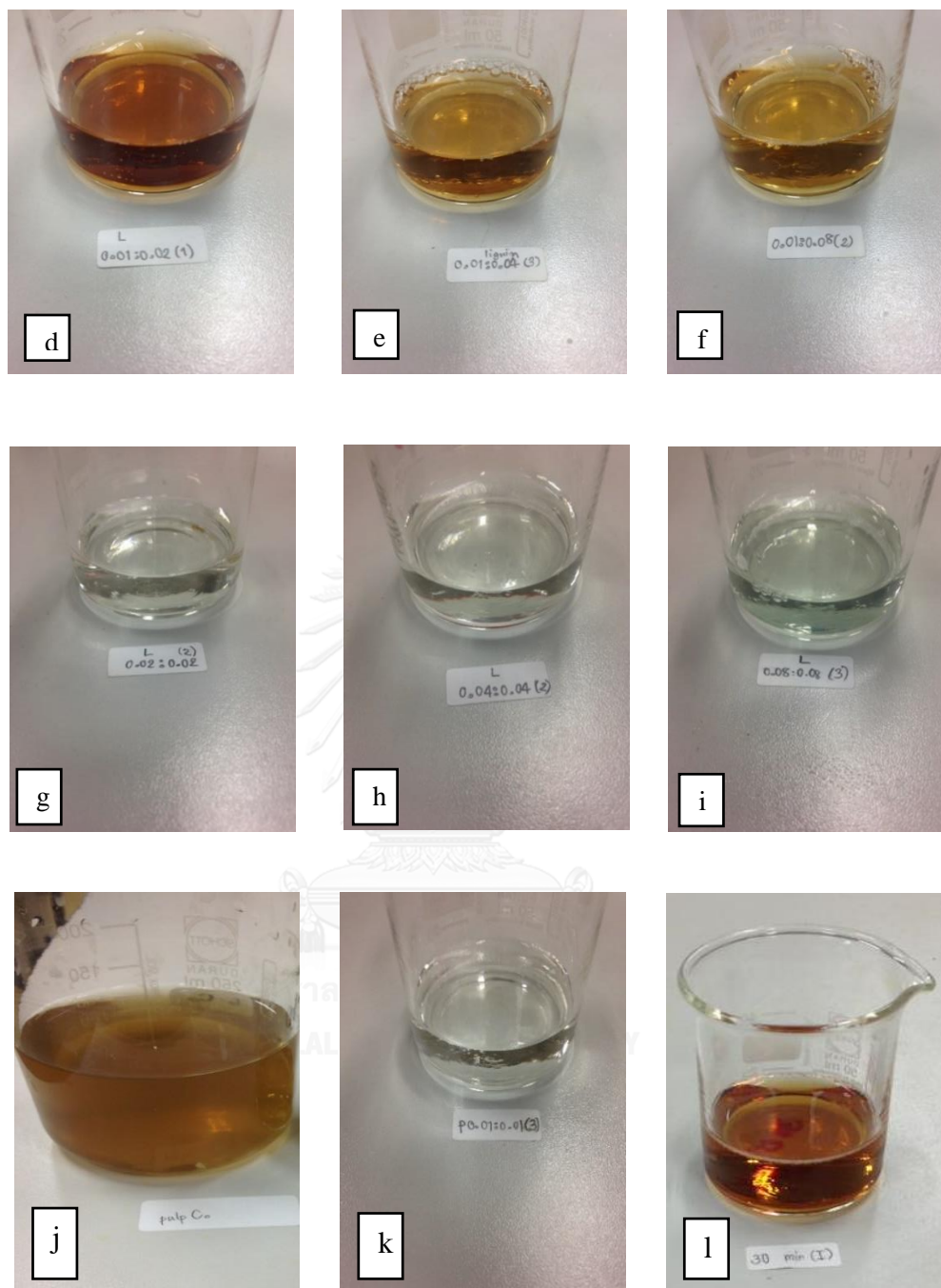


**Figure B-2** Color removal by reductive precipitation in (a) 1 g/L lignin, (b) L0.01:0.0005, (c) L0.01:0.01, (d) L0.01:0.02, (e) L0.01:0.04, (f) L0.01:0.08, (g) L0.02:0.02, (h) L0.04:0.04, (i) L0.08:0.08, (j) initial pulp wastewater, (k) P 0.01:0.01, and (l) 1 g/L nZVI commercial.

**Appendix C: Calibration curve of lignin, iron, arsenic, and hydrogen production.**

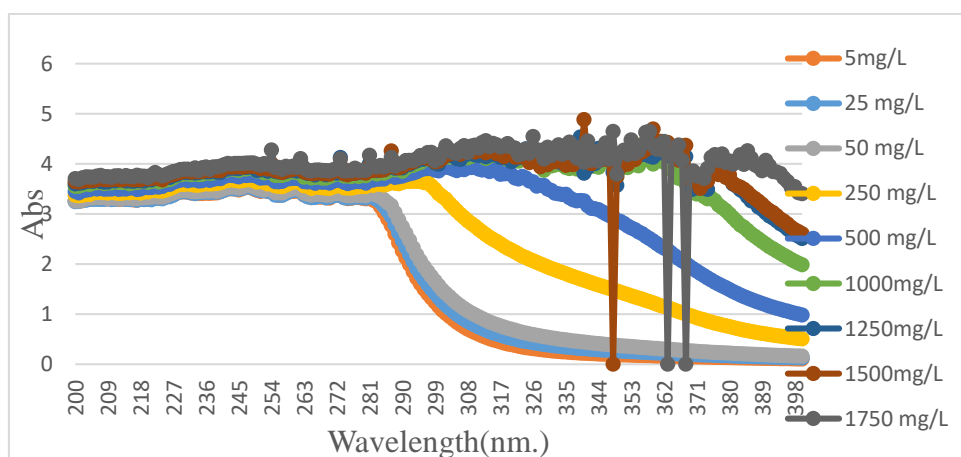


**Figure C-1** Wavelength and absorbance of various lignin concentrations.

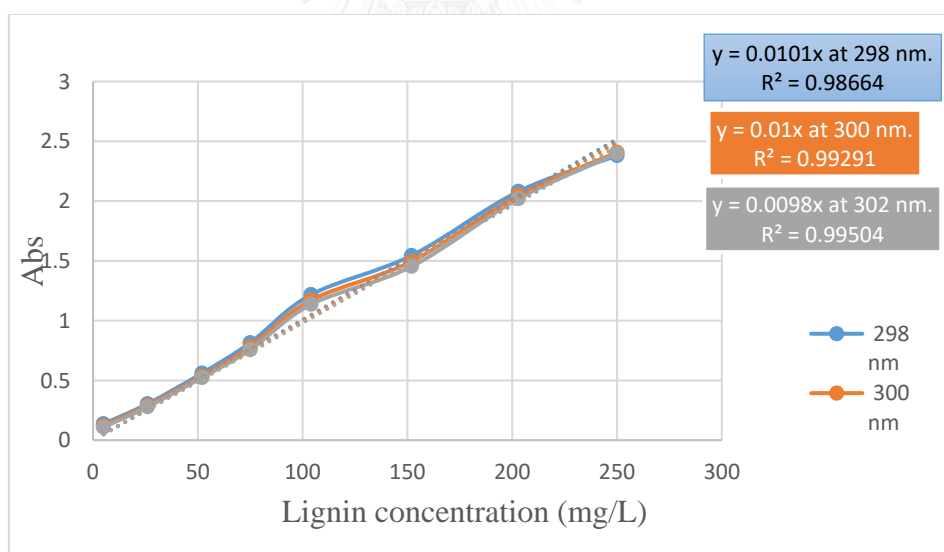


**Figure C-2** Calibration curve of lignin concentration at wavelength at 298, 300, 302 nm.

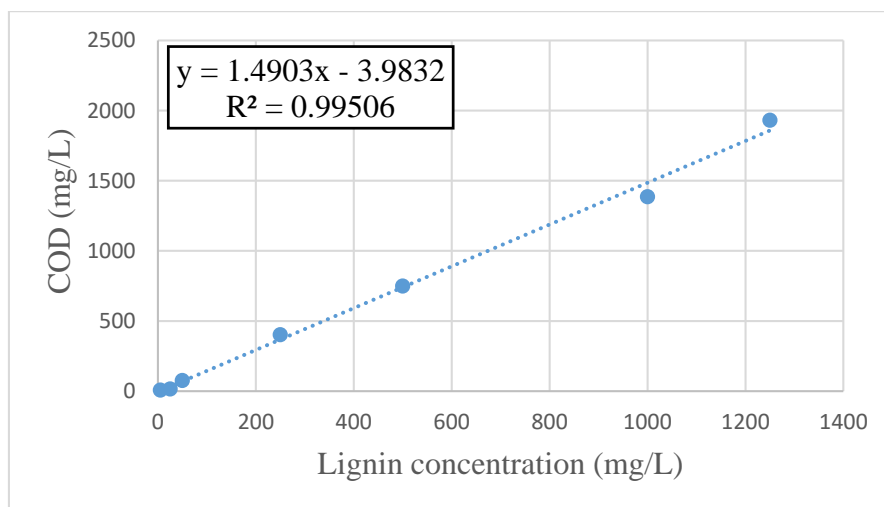


**Figure C-3** COD of lignin concentration by using closed reflux, titrimetric method.

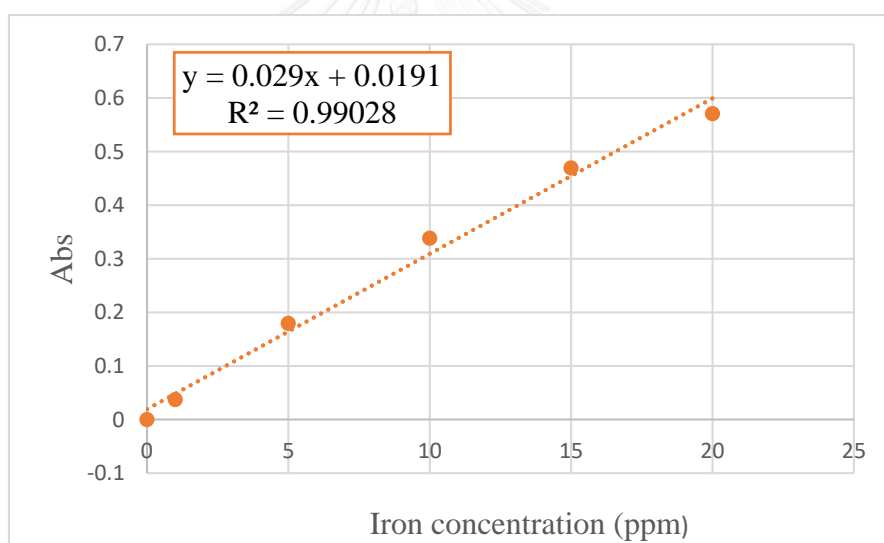


**Figure C-4** Calibration curve of iron concentration (ppm) by using FAAS.

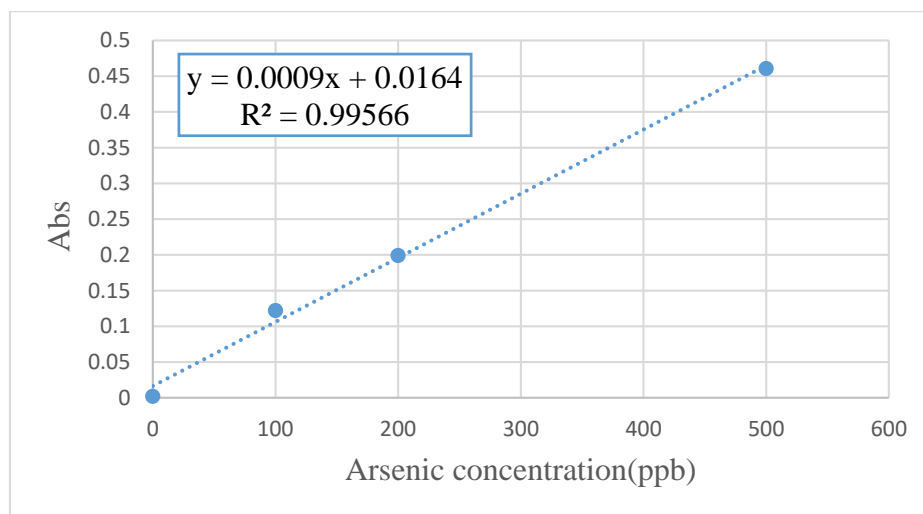


**Figure C-5** Calibration curve of arsenic concentration (ppb) by using GAAS.

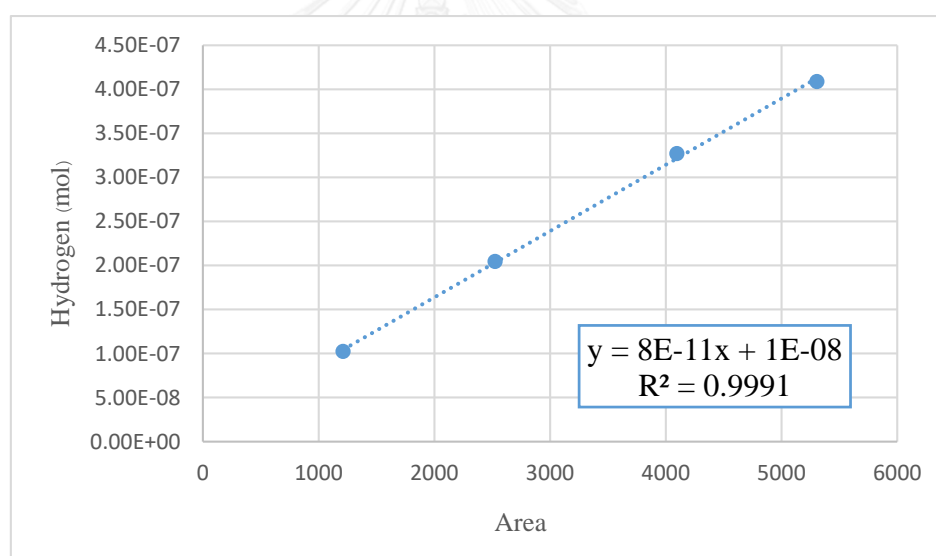


**Figure C-6** Calibration curve of hydrogen (mole) by using GC-TCD.

## VITA

Mr. Phoomipat Jungcharoen was born on June 11, 1992 in Chonburi, Thailand. He graduated with a bachelor's degree in Environmental Engineering from King Mongkut's University of Technology Thonburi in April of 2015, and received a full scholarship to study for his master's degree in Hazardous Substance and Environmental Management, at Chulalongkorn University in June of 2015.

